Universität Regensburg
Mathematik

Numerical Approximation of Anisotropic Geometric Evolution Equations

John W. Barrett, Harald Garcke and Robert Nürnberg

Preprint Nr. 09/2006

Numerical Approximation of Anisotropic Geometric Evolution Equations

John W. Barrett[†] Harald Garcke[‡] Robert Nürnberg[†]

Abstract

We present a variational formulation of fully anisotropic motion by surface diffusion and mean curvature flow, as well as related flows. The proposed scheme covers both the closed curve case, and the case of curves that are connected via triple junction points. On introducing a parametric finite element approximation, we prove stability bounds and report on numerical experiments, including crystalline mean curvature flow and crystalline surface diffusion. The presented scheme has very good properties with respect to the equidistribution of mesh points and, if applicable, area conservation.

Key words. anisotropic surface diffusion, mean curvature flow, crystalline surface energy, triple junctions, parametric finite elements, Schur complement, tangential movement

AMS subject classifications. 65M60, 65M12, 35K55, 53C44, 74E10, 74E15

1 Introduction

Geometric flows, in which hypersurfaces move such that an anisotropic surface energy decreases, appear in many situations in the natural sciences and in geometry. E.g. in materials science one observes that the surface energy density of a crystal surface depends locally on the normal to the surface. Often physical evolution laws tend to decrease the energy and the easiest law to decrease anisotropic surface energy is motion by anisotropic mean curvature flow, which generalizes the classical mean curvature flow $\mathcal{V} = \varkappa$, where $\mathcal{V}$ is the normal velocity and $\varkappa$ is the mean curvature, i.e. the sum of the principal curvatures. If the enclosed volume is preserved, then possible evolution laws that decrease the anisotropic surface energy are volume preserving anisotropic mean curvature flow and anisotropic surface diffusion. In the volume preserving anisotropic mean curvature flow a

[†]Department of Mathematics, Imperial College, London, SW7 2AZ, U.K.
[‡]NWF I – Mathematik, Universität Regensburg, 93040 Regensburg, Germany

time dependent but spatially constant term is added to the curvature flow equation, such that volume is preserved. Hence this flow is of second order, like the mean curvature flow. The anisotropic surface diffusion law generalizes isotropic surface diffusion,

$$\mathcal{V} = -\Delta_s \varkappa\,,$$

where Δ_s is the Laplace–Beltrami operator on the surface. Since one needs four spatial derivatives to compute $\Delta_s \varkappa$, this flow is of fourth order. We refer to the papers Wulff (1901), Herring (1951), Frank (1963), Taylor, Cahn, and Handwerker (1992) and Taylor and Cahn (1994) for more details on anisotropy in materials science and geometry, and we refer to Taylor and Cahn (1994) for volume preserving geometric flows.

In the recent papers Barrett, Garcke, and Nürnberg (2005) and Barrett, Garcke, and Nürnberg (2006a), the authors introduced a parametric finite element approximation for the evolution of closed curves and curve networks under motion by isotropic surface diffusion and mean curvature, as well as related (isotropic) evolution laws. In this paper we will show that these approximations can be adapted to yield stable and efficient schemes for geometric evolution laws governed by anisotropic surface energies.

An anisotropic surface energy has the form

$$|\Gamma|_\gamma := \int_\Gamma \gamma(\vec{\nu})\,\mathrm{d}s, \tag{1.1}$$

where $\Gamma \subset \mathbb{R}^d$, $d = 2, 3$, is a hypersurface with unit normal $\vec{\nu}$ and $\gamma : \mathbb{R}^d \setminus \{\vec{0}\} \to \mathbb{R}_{>0}$ is a given anisotropy function. The function γ is positively homogeneous of degree one, i.e.

$$\gamma(\lambda\,\vec{p}) = |\lambda|\,\gamma(\vec{p}) \quad \forall\ \vec{p} \in \mathbb{R}^d,\ \forall\ \lambda \in \mathbb{R} \setminus \{0\} \quad \Rightarrow \quad \gamma'(\vec{p})\,.\,\vec{p} = \gamma(\vec{p}) \quad \forall\ \vec{p} \in \mathbb{R}^d, \tag{1.2}$$

where γ' is the gradient of γ. In the isotropic case we have that $\gamma(\vec{p}) = |\vec{p}|$ and so $\gamma(\vec{\nu}) = 1$, which means that $|\Gamma|_\gamma$ reduces to $|\Gamma|$, the surface area of Γ. A wide class of anisotropies can be modelled by

$$\gamma(\vec{p}) = \sum_{\ell=1}^{L} \gamma^{(\ell)}(\vec{p}) = \sum_{\ell=1}^{L} \sqrt{\vec{p}\,.\,G^{(\ell)}\,\vec{p}} \qquad \Rightarrow \qquad \gamma'(\vec{p}) = \sum_{\ell=1}^{L} [\gamma^{(\ell)}(\vec{p})]^{-1}\,G^{(\ell)}\,\vec{p}\,, \tag{1.3}$$

where $G^{(\ell)} \in \mathbb{R}^{d\times d}$, $\ell = 1 \to L$, are symmetric and positive definite; and in this paper we will restrict our analysis to anisotropies of the form (1.3). This will enable us to prove stability bounds for our fully discrete (parametric) approximations for anisotropic geometric evolution laws, something that is new in the literature. We remark that variants of our proposed schemes can be used for anisotropies that are more general than (1.3), but it does not seem to be possible to prove analogue stability results in these more general situations. Examples for energies of the form (1.3) are $\gamma(\vec{p}) = \left[\sum_{i=1}^{d} \alpha_i^2\,p_i^2\right]^{\frac{1}{2}}$, where $\vec{\alpha} \in \mathbb{R}^d_{>0}$ is given, and the regularized l^1 norm

$$\gamma(\vec{p}) = \sum_{i=1}^{d} \sqrt{\varepsilon^2\,|\vec{p}|^2 + p_i^2} \tag{1.4}$$

that was, for instance, considered in Deckelnick, Dziuk, and Elliott (2005a). For more details on possible anisotropy functions, see Bellettini and Paolini (1996). Different anisotropies can be visualized by their Frank diagram

$$\mathcal{F} := \{\vec{p} \in \mathbb{R}^d : \gamma(\vec{p}) \leq 1\}$$

and their Wulff shape

$$\mathcal{W} := \{\vec{q} \in \mathbb{R}^d : \gamma^*(\vec{q}) \leq 1\},$$

which was first introduced by Wulff (1901). Here γ^* is the dual to γ and is defined by

$$\gamma^*(\vec{q}) = \sup_{\vec{p} \in \mathbb{R}^d \setminus \{\vec{0}\}} \frac{\vec{p}\,.\,\vec{q}}{\gamma(\vec{p})}.$$

It follows immediately from the above definition that Wulff shapes are convex. We note that the Frank diagrams for (1.3) are always convex.

As the anisotropy (1.3) satisfies $\vec{p}\,.\,\gamma'(\vec{q}) \leq \gamma(\vec{p})$ for all $\vec{p}$, $\vec{q} \in \mathbb{R}^d \setminus \{\vec{0}\}$, it is straightforward to construct the Wulff shape $\mathcal{W}$ and find γ^*. Let S^{d-1} be the unit sphere in $\mathbb{R}^d$. Then

$$\vec{r}_{\mathcal{F}}(\vec{r}) := [\gamma(\vec{r})]^{-1}\,\vec{r} \qquad \text{and} \qquad \vec{r}_{\mathcal{W}}(\vec{r}) := \gamma'(\vec{r}), \qquad \vec{r} \in S^{d-1}, \tag{1.5}$$

parameterize the boundaries of $\mathcal{F}$ and $\mathcal{W}$, respectively. Moreover, $\gamma^*(\vec{q}) = |\vec{r}_{\mathcal{W}}(\vec{r})|^{-1}$ if $\gamma'(\vec{r})$ and $\vec{q} \in S^{d-1}$ point in the same direction. This defines γ^* for $\vec{q} \in S^{d-1}$, and via the 1-homogeneity on all of $\mathbb{R}^d \setminus \{\vec{0}\}$. In fact one can show that

$$\gamma^*(\vec{q}) = \sqrt{\vec{q}\,.\,G^*_{\vec{q}}\,\vec{q}} \qquad \text{with} \qquad G^*_{\vec{q}} = \left(\sum_{\ell=1}^{L} \mu^{(\ell)}(\vec{q})\, G^{(\ell)}\right)^{-1}, \tag{1.6}$$

where $\sum_{\ell=1}^{L} [\mu^{(\ell)}(\vec{q})]^{-1} = 1$ and $\mu^{(\ell)}(\vec{q}) > 1$, $\ell = 1 \to L$. For more details on ways to construct the Wulff shape for a given anisotropy γ, see Peng, Osher, Merriman, and Zhao (1999).

In Figure 1 we give the Frank diagrams in $\mathbb{R}^2$ for anisotropies of the form (1.3); in particular for

$$\gamma(\vec{p}) = \sum_{\ell=1}^{L} \sqrt{\vec{p}\,.\,R(-\theta_\ell) D(\varepsilon_\ell) R(\theta_\ell)\,\vec{p}}, \qquad \text{where } D(\varepsilon) := \begin{pmatrix} 1 & 0 \\ 0 & \varepsilon^2 \end{pmatrix} \tag{1.7}$$

and $R(\theta) := \begin{pmatrix} \cos\theta & \sin\theta \\ -\sin\theta & \cos\theta \end{pmatrix}$ is a clockwise rotation matrix through the given angle θ. For the anisotropies in Figure 1 we used $\varepsilon_\ell^2 \equiv 10^{-2}$ and $\varepsilon_\ell^2 \equiv 10^{-5}$, respectively, with $(\theta_1, \ldots, \theta_L) = (0, \frac{\pi}{2})$, $(0, \frac{\pi}{3}, \frac{2\pi}{3})$, $(0, \frac{\pi}{4}, \frac{\pi}{2}, \frac{3\pi}{4})$, $(0, \frac{\pi}{3}, \frac{\pi}{4})$ and $(0, \frac{\pi}{10}, \frac{\pi}{9}, \frac{3\pi}{4})$. Note that for the last two choices the Frank diagrams have got only a two-fold symmetry. The Frank diagrams for the same anisotropies, but with $\varepsilon_1^2 = 0.1$ and $\varepsilon_\ell^2 = 10^{-5}$, $\ell = 2 \to L$ can be seen in Figure 2. Finally, the corresponding Wulff shapes are presented in Figures 3.

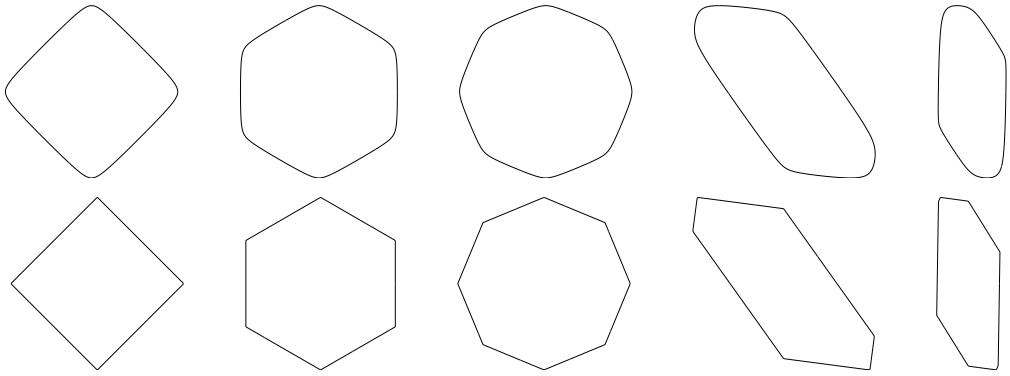

Figure 1: Frank diagrams for different choices of (1.3).

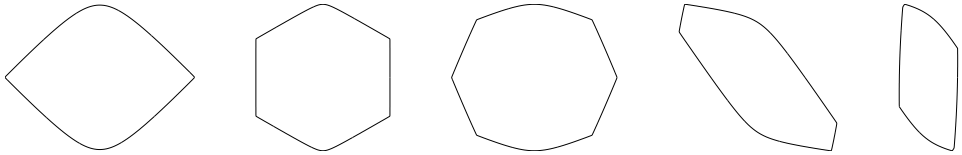

Figure 2: Frank diagrams for different choices of (1.3).

Given an anisotropy γ, the so called Cahn–Hoffmann vector is defined by

$$\vec{\nu}_\gamma := \gamma'(\vec{\nu})\,,$$

where $\vec{\nu} \in \mathbb{R}^d$ is the unit normal to $\Gamma \subset \mathbb{R}^d$, see Cahn and Hoffmann (1974). Note that in the isotropic case, $\gamma(\vec{p}) = |\vec{p}|$, we have that $\vec{\nu}_\gamma \equiv \vec{\nu}$. Then the weighted mean curvature is given by

$$\varkappa_\gamma := -\nabla_s \,.\, \vec{\nu}_\gamma\,; \tag{1.8}$$

where $\nabla_s \,.$ is the tangential divergence on Γ, with $\nabla_s f = \nabla f - (\vec{\nu} \,.\, \nabla f)\,\vec{\nu}$ being the tangential gradient on Γ; see e.g. Deckelnick, Dziuk, and Elliott (2005a, p. 150). Here we have adopted the opposite sign convention to that in Deckelnick, Dziuk, and Elliott (2005a), in that in the isotropic case the mean curvature $\varkappa := -\nabla_s \,.\, \vec{\nu}$ is positive if the curvature is in the direction of the normal. Although the sign of $\varkappa_\gamma$ depends on the choice of $\vec{\nu}$, the weighted mean curvature vector $\varkappa_\gamma\,\vec{\nu}$ is invariant of this choice.

Motion by anisotropic mean curvature and anisotropic surface diffusion are then given by

$$\text{(a)} \quad \mathcal{V} = \varkappa_\gamma \qquad \text{and} \qquad \text{(b)} \quad \mathcal{V} = -\Delta_s\,\varkappa_\gamma, \tag{1.9}$$

respectively, where $\mathcal{V}$ is the normal velocity of Γ and Δ_s is the surface Laplacian. It is also possible to include an anisotropic mobility into (1.9a,b), leading to:

$$\text{(a)} \quad \mathcal{V} = \beta(\vec{\nu})\,\varkappa_\gamma\,, \qquad \text{and} \qquad \text{(b)} \quad \mathcal{V} = -\nabla_s \,.\, (\beta(\vec{\nu})\,\nabla_s\,\varkappa_\gamma)\,, \tag{1.10}$$

where $\beta : S^{d-1} \to \mathbb{R}$ is a given smooth positive function. For a derivation of (1.10a), we refer to Angenent and Gurtin (1989) and Gurtin (1993); see also Taylor, Cahn, and

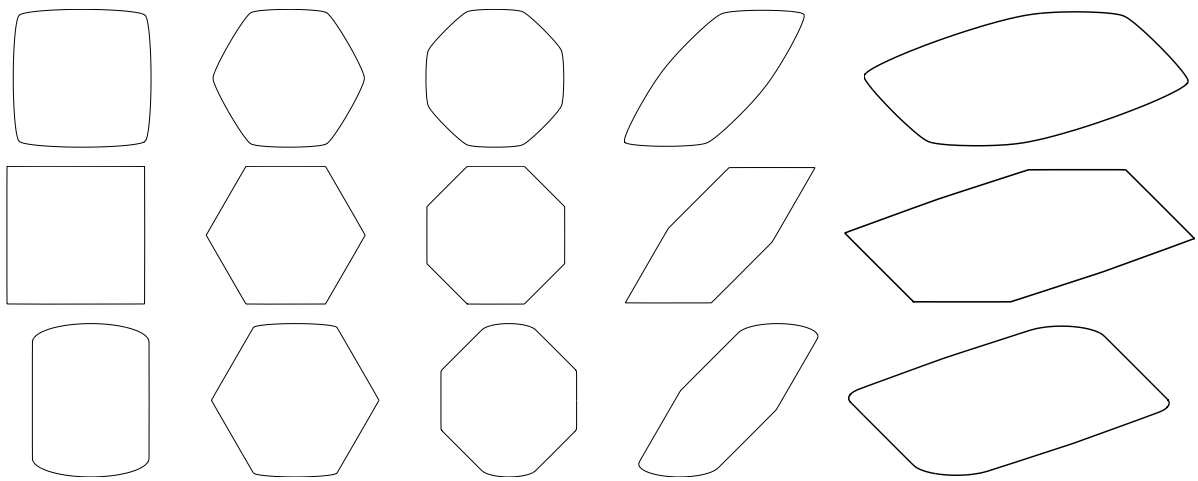

Figure 3: Wulff shapes for the Frank diagrams in Figures 1 and 2.

Handwerker (1992). We remark that the algorithms we present in this paper can easily be generalized to study nonlinear relations between $\mathcal{V}$ and $\varkappa_\gamma$ of the form

$$\mathcal{V} = \beta(\vec{\nu})\, f(\varkappa_\gamma)\,, \tag{1.11}$$

where f is a strictly monotonically increasing continuous function. Of particular interest is the case $f(r) = -r^{-1}$, i.e. the inverse anisotropic mean curvature flow, see Barrett, Garcke, and Nürnberg (2006a) for the relevant details in the isotropic case.

Given a parameterization $\vec{x} \in \mathbb{R}^d$ of Γ, (1.10a,b) can be formulated as

$$\text{(a)} \quad \vec{x}_t \,.\, \vec{\nu} = \beta(\vec{\nu})\, \varkappa_\gamma \qquad \text{and} \qquad \text{(b)} \quad \vec{x}_t \,.\, \vec{\nu} = -\nabla_s \,.\, (\beta(\vec{\nu})\, \nabla_s\, \varkappa_\gamma)\,, \tag{1.12}$$

respectively. It follows from (1.8), see e.g. Deckelnick, Dziuk, and Elliott (2005a, p. 194), that

$$\varkappa_\gamma\, \vec{\nu} = -\nabla_s \,.\, (\vec{\nu}\, [\gamma'(\vec{\nu})]^T) + \nabla_s \,.\, (\gamma(\vec{\nu})\, \nabla_s\, \vec{x}) + \gamma(\vec{\nu})\, \Delta_s\, \vec{x}\,. \tag{1.13}$$

Here $\nabla_s\, \vec{\varphi} \in \mathbb{R}^{d\times d}$ with $(\nabla_s\, \vec{\varphi})_{kl} = [\nabla_s\, \varphi_k]_l$, $k, l = 1 \to d$, for $\vec{\varphi} = (\varphi_1, \ldots, \varphi_d)^T \in \mathbb{R}^d$; and $\nabla_s \,.\, A \in \mathbb{R}^d$ with $[\nabla_s \,.\, A]_l = \nabla_s \,.\, \vec{A}_l$, $l = 1 \to d$, for $A = [\vec{A}_1 \ldots \vec{A}_d] \in \mathbb{R}^{d\times d}$. We define also $A \,.\, B := \sum_{k,l=1}^d A_{kl}\, B_{kl}$ for $A, B \in \mathbb{R}^{d\times d}$.

We remark that the tangential component $\vec{x}_t - (\vec{x}_t \,.\, \vec{\nu})\, \vec{\nu}$ of the velocity $\vec{x}_t$ is not prescribed in (1.12a,b), similarly to the formulations of the isotropic evolution equations in Barrett, Garcke, and Nürnberg (2005) and Barrett, Garcke, and Nürnberg (2006a). Hence (1.12a,b) with (1.13) admit a whole family of solutions $\vec{x}$; although the evolution of the hypersurface Γ is uniquely defined.

We now assume that Γ is compact, so by the Jordan–Brouwer decomposition theorem it is the boundary of an open bounded subset of $\mathbb{R}^d$. Testing (1.12a,b) and (1.13) with suitable smooth functions φ and $\vec{\varphi}$, and applying the Gauss theorem on manifolds,

$\int_\Gamma \nabla_s \,.\, \vec{g}\,\mathrm{d}s = -\int_\Gamma \varkappa\,\vec{g}\,.\,\vec{\nu}\,\mathrm{d}s$, yields, on noting that $\nabla_s\, g\,.\,\vec{\nu} = 0$, that

$$\int_\Gamma \vec{x}_t\,.\,\vec{\nu}\,\varphi\,\mathrm{d}s = \int_\Gamma \beta(\vec{\nu})\,\varkappa_\gamma\,\varphi\,\mathrm{d}s \quad \text{or} \quad \int_\Gamma \vec{x}_t\,.\,\vec{\nu}\,\varphi\,\mathrm{d}s = \int_\Gamma \beta(\vec{\nu})\,\nabla_s\,\varkappa_\gamma\,.\,\nabla_s\,\varphi\,\mathrm{d}s, \tag{1.14a}$$

$$\text{and} \quad \int_\Gamma \varkappa_\gamma\,\vec{\nu}\,.\,\vec{\varphi}\,\mathrm{d}s = \int_\Gamma [\vec{\nu}\,[\gamma'(\vec{\nu})]^T\,]\,.\,\nabla_s\,\vec{\varphi}\,\mathrm{d}s - \int_\Gamma \gamma(\vec{\nu})\,\nabla_s\,\vec{x}\,.\,\nabla_s\,\vec{\varphi}\,\mathrm{d}s; \tag{1.14b}$$

see e.g. once again Deckelnick, Dziuk, and Elliott (2005a, p. 194) for the details in deriving (1.14b). For $d = 2$ we note that (1.13) collapses to $\varkappa_\gamma\,\vec{\nu} = [\gamma'(\vec{\nu})]_s^\perp$, and so equation (1.14b) can be rewritten as

$$\int_\Gamma \varkappa_\gamma\,\vec{\nu}\,.\,\vec{\varphi}\,\mathrm{d}s = \int_\Gamma \gamma'(\vec{\nu})\,.\,\vec{\varphi}_s^{\,\perp}\,\mathrm{d}s\,, \tag{1.15}$$

where $\vec{p}^{\,\perp} := R(\frac{\pi}{2})\,\vec{p}$ denotes the clockwise rotation by $\frac{\pi}{2}$; see e.g. once again Deckelnick, Dziuk, and Elliott (2005a, p. 196) for the details.

As remarked earlier, a surface that encloses a region in $\mathbb{R}^d$ and evolves according to anisotropic surface diffusion conserves volume. Choosing $\vec{\nu}$ to be the outward unit normal to the region and taking $a(t)$ as the total enclosed volume, this follows from

$$\frac{d}{dt}\,a(t) = \int_\Gamma \mathcal{V}\,\mathrm{d}s = \int_\Gamma \vec{x}_t\,.\,\vec{\nu}\,\mathrm{d}s = 0;$$

where the last identity follows from the second equation in (1.14a) with $\varphi \equiv 1$. Furthermore the total surface energy, $|\Gamma(t)|_\gamma$, decreases in time, as choosing $\varphi = \varkappa_\gamma$ in the second equation in (1.14a) yields that

$$\frac{d}{dt}\,|\Gamma(t)|_\gamma = -\int_\Gamma \varkappa_\gamma\,\mathcal{V}\,\mathrm{d}s = -\int_\Gamma \varkappa_\gamma\,\vec{x}_t\,.\,\vec{\nu}\,\mathrm{d}s = -\int_\Gamma \beta(\vec{\nu})\,(\nabla_s\,\varkappa_\gamma)^2\,\mathrm{d}s \leq 0. \tag{1.16}$$

An analogue of (1.16) also holds for anisotropic mean curvature flow, (1.10a). A version of (1.10a) that preserves the enclosed volume is given by

$$\mathcal{V} = \beta(\vec{\nu})\,\varkappa_\gamma - \frac{\int_\Gamma \beta(\vec{\nu})\,\varkappa_\gamma\,\mathrm{d}s}{\int_\Gamma 1\,\mathrm{d}s}, \tag{1.17}$$

the so called conserved (anisotropic) mean curvature flow, also called (anisotropic) surface attachment limited kinetics (SALK). An intermediate law between (1.17) and (1.10b) is the following evolution law:

$$\mathcal{V} = -\nabla_s\,.\,(\beta(\vec{\nu})\,\nabla_s\,[\mathcal{L}^{-1}\,(\beta(\vec{\nu})\,\varkappa_\gamma\,)\,]\,), \quad \text{where} \quad \mathcal{L}\,g := -\tfrac{1}{\xi}\,\nabla_s\,.\,(\beta(\vec{\nu})\,\nabla_s\,g\,) + \tfrac{1}{\alpha}\,\beta(\vec{\nu})\,g \tag{1.18}$$

and $\alpha, \xi \in \mathbb{R}_{>0}$. The flow (1.18), in the isotropic case with $\beta \equiv 1$, was first discussed in Taylor and Cahn (1994); see also Elliott and Garcke (1997). It is similar to (1.17) and (1.10b) in that the enclosed volume is conserved, while the surface energy $|\Gamma|_\gamma$ decreases. We observe that for $\alpha \to \infty$ and $\xi = 1$, the solutions to (1.18) should converge to

solutions of (1.17), while $\xi \to \infty$ and $\alpha = 1$ corresponds to the law (1.10b). Given a parameterization $\vec{x} \in \mathbb{R}^d$ of Γ, (1.18) can be written as a system of second order equations:

$$\vec{x}_t \,.\, \vec{\nu} = -\nabla_s \,.\, (\beta(\vec{\nu})\, \nabla_s\, y\,)\,, \qquad \mathcal{L}\, y = \beta(\vec{\nu})\, \varkappa_\gamma\,, \qquad \text{and (1.13).} \tag{1.19}$$

In Section 2, we will consider a finite element approximation of a variational formulation of (1.19), as well as (1.12a,b) with (1.13).

Theoretical aspects of anisotropic mean curvature flow were studied in Taylor (1992), Bellettini and Paolini (1996), and Giga (2006). For nondifferentiable surface energies γ one can introduce the notion of crystalline curvature flow, which was first considered in Taylor (1988) and Angenent and Gurtin (1989), and was later also studied in Girão (1995). Crystalline surface diffusion was studied in Taylor (1996) and Taylor (2002). Crystalline motion including triple junctions was considered in Taylor (1993) and Taylor (1999). In this paper we will only consider smooth anisotropies, but the Frank diagrams displayed in Figures 1 and 2 show that we can approximate crystalline surface energies very accurately.

A parametric finite element approximation of anisotropic mean curvature flow was studied in Clarenz, Dziuk, and Rumpf (2003), while a level set formulation for anisotropic mean curvature flow and surface diffusion was discussed in Clarenz, Haußer, Rumpf, Voigt, and Weikard (2005). A different level set formulation of anisotropic surface diffusion was considered in Chopp and Sethian (1999), see also Russo and Smereka (2000). A finite element formulation of anisotropic mean curvature flow was considered in Deckelnick and Dziuk (2003). Anisotropic surface diffusion for graphs was considered in Deckelnick, Dziuk, and Elliott (2005b). A parametric approximation for a regularized version of anisotropic mean curvature flow, that was introduced by Di Carlo, Gurtin, and Podio-Guidugli (1992), of curves, that is based on the scheme in Bänsch, Morin, and Nochetto (2005), was considered in Haußer and Voigt (2006) and extended to regularized anisotropic surface diffusion and related flows in Haußer and Voigt (2005). A phase field model for anisotropic surface diffusion, including approximative crystalline surface diffusion, in the context of epitaxial growth is considered in Barrett, Garcke, and Nürnberg (2006b). A phase field model for curve networks moving under motion by anisotropic mean curvature was considered in Garcke, Nestler, and Stoth (1999).

From now on, and throughout this paper, we will restrict ourselves to the case $d = 2$, i.e. the evolution of curves in the plane. In many applications, networks of curves with triple junctions appear. A model for (isotropic) surface diffusion of a network of curves has been introduced by Garcke and Novick-Cohen (2000), and this can be naturally generalized to anisotropic surface energies. In the following, we describe this model for a network of three curves. Let Γ_1, Γ_2, Γ_3 be the given curves in $\mathbb{R}^d$, $d = 2$, with anisotropies $\gamma_i(\vec{\nu}_i)$ of the form (1.3), $i = 1 \to 3$, that intersect at two triple junction points Λ_1 and Λ_2; see Figure 4. Let $\vec{\tau}_i \in \mathbb{R}^d$ be the unit tangent to Γ_i pointing away from the triple junction point Λ_1 and towards point Λ_2, and let $\vec{\nu}_i = -\vec{\tau}_i^{\,\perp} \in \mathbb{R}^d$ be the unit normal to Γ_i. Then the normal velocity for each curve is given by

$$\mathcal{V}_i = -\nabla_s \,.\, (\beta_i(\vec{\nu}_i)\, \nabla_s\, \varkappa_{\gamma,i}), \qquad i = 1 \to 3, \tag{1.20}$$

where $\varkappa_{\gamma,i} = -\nabla_s \,.\, [\gamma_i'(\vec{\nu}_i)]$ is the weighted mean curvature of Γ_i, i.e. the analogue of (1.8),

and $\beta_i(\vec{\nu}_i)$ is a positive mobility. Then, in addition to (1.20), the following conditions have to hold at the triple junction points Λ_1 and Λ_2:

$$\text{the triple junction does not pull apart,} \tag{1.21a}$$
$$\gamma_1'(\vec{\nu}_1) + \gamma_2'(\vec{\nu}_2) + \gamma_3'(\vec{\nu}_3) = \vec{0}, \tag{1.21b}$$
$$\vec{\tau}_1 \,.\, \beta_1(\vec{\nu}_1)\, \nabla_s\, \varkappa_{\gamma,1} = \vec{\tau}_2 \,.\, \beta_2(\vec{\nu}_2)\, \nabla_s\, \varkappa_{\gamma,2} = \vec{\tau}_3 \,.\, \beta_3(\vec{\nu}_3)\, \nabla_s\, \varkappa_{\gamma,3}, \tag{1.21c}$$
$$\varkappa_{\gamma,1} + \varkappa_{\gamma,2} + \varkappa_{\gamma,3} = 0, \tag{1.21d}$$

where $\nabla_s\,|_{\Gamma_i} \equiv \vec{\tau}_i\, \frac{\partial}{\partial s}$ with s being the arclength. The conditions (1.21a–d) are an attachment condition, a force balance condition, a flux balance condition and a chemical potential continuity condition, respectively. We note that (1.21b) leads to angle conditions at the triple junction, and reduces to the well-known Young's law in the isotropic case. The flux balance condition (1.21c) follows from mass balance considerations at the triple junction. In order to be in thermodynamical equilibrium locally, it is necessary that the chemical potential differences are continuous which leads to (1.21d); for more details on the above derivations in the isotropic case see Garcke and Novick-Cohen (2000).

Taking the boundary conditions (1.21a–d) into account, we easily derive that the total area of the enclosed phases are conserved; e.g. for the area $a_3(t)$ of the phase enclosed by Γ_1 and Γ_2, see Figure 4, we obtain that

$$\begin{aligned}\frac{d}{dt}\, a_3(t) &= \int_{\Gamma_2} \mathcal{V}_2 \,\mathrm{d}s - \int_{\Gamma_1} \mathcal{V}_1 \,\mathrm{d}s \\ &= -\int_{\Gamma_2} \nabla_s \,.\, (\beta_2(\vec{\nu}_2)\, \nabla_s\, \varkappa_{\gamma,2}) \,\mathrm{d}s + \int_{\Gamma_1} \nabla_s \,.\, (\beta_1(\vec{\nu}_1)\, \nabla_s\, \varkappa_{\gamma,1}) \,\mathrm{d}s = 0,\end{aligned}$$

where the last identity follows from (1.21c). The total free energy of the system is given by $\sum_{i=1}^{3} |\Gamma_i(t)|_\gamma$, where $|\Gamma_i(t)|_\gamma$ is now the weighted length of $\Gamma_i(t)$, and we obtain from

$$\begin{aligned}\frac{d}{dt} \sum_{i=1}^{3} |\Gamma_i(t)|_\gamma &= -\sum_{i=1}^{3} \int_{\Gamma_i} \varkappa_{\gamma,i}\, \mathcal{V}_i \,\mathrm{d}s = \sum_{i=1}^{3} \int_{\Gamma_i} \varkappa_{\gamma,i}\, \nabla_s \,.\, (\beta_i(\vec{\nu}_i)\, \nabla_s\, \varkappa_{\gamma,i}) \,\mathrm{d}s \\ &= -\sum_{i=1}^{3} \int_{\Gamma_i} \beta_i(\vec{\nu}_i)\, |\nabla_s\, \varkappa_{\gamma,i}|^2 \,\mathrm{d}s \leq 0\end{aligned}$$

that the total free energy cannot increase. The first identity above holds because of (1.21b), and the last identity is true since the boundary conditions (1.21c) and (1.21d) imply that the boundary terms arising from the integration by parts disappear.

For parameterizations $\vec{x}_i \in \mathbb{R}^d$ of Γ_i, $i = 1 \to 3$, (1.20) can be written as a system of second order equations:

$$(\vec{x}_i)_t \,.\, \vec{\nu}_i = -\nabla_s \,.\, (\beta_i(\vec{\nu}_i)\, \nabla_s\, \varkappa_{\gamma,i}), \qquad \varkappa_{\gamma,i}\, \vec{\nu}_i = [\gamma_i'(\vec{\nu}_i)]_s^\perp. \tag{1.22}$$

A variational formulation of (1.22) and (1.21a–d) will form the basis for our scheme that we present in Section 2. We note that for the isotropic case, the second equation in (1.22) collapses to $\varkappa_i\, \vec{\nu}_i = [\vec{\nu}_i]_s^\perp = [\vec{\tau}_i]_s = \Delta_s\, \vec{x}_i$.

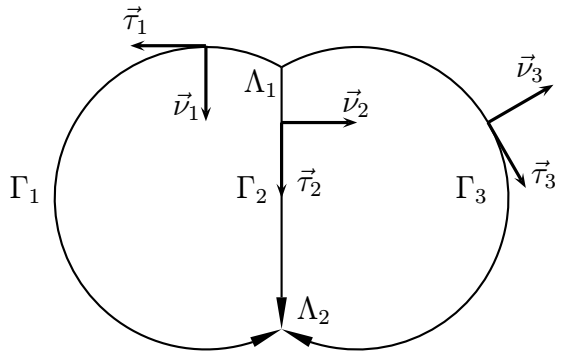

Figure 4: The setup of $\Gamma = (\Gamma_1, \Gamma_2, \Gamma_3)$.

In the recent paper Barrett, Garcke, and Nürnberg (2006a), the authors considered also the possibility of curve intersections with a fixed external domain boundary $\partial\Omega$, where Ω is a domain in $\mathbb{R}^d$; see Figure 5 for an example. As we will consider this situation also for the anisotropic evolution laws in this paper, we now state the necessary conditions that have to hold at these intersections. Let $\partial\Omega$ be given by a function $F \in C^1(\mathbb{R}^d)$ such that

$$\partial\Omega = \{\vec{z} \in \mathbb{R}^d : F(\vec{z}) = 0\} \qquad \text{and} \qquad |\nabla F(\vec{z})| = 1 \quad \forall\ \vec{z} \in \partial\Omega\,. \tag{1.23}$$

Then, for the three given curves Γ_i, $i = 1 \to 3$, the conditions (1.21a–d) only need to hold at the triple junction $\Lambda = \vec{x}_i(0)$, $i = 1 \to 3$, while at the boundary intersection points $\vec{x}_i(1)$, $i = 1 \to 3$, the following conditions have to hold:

$$\text{the curve endpoint remains attached to } \partial\Omega, \tag{1.24a}$$

$$[\gamma_i'(\vec{\nu}_i)]^\perp \,.\, [\nabla F(\vec{x}_i(1))]^\perp = 0, \tag{1.24b}$$

$$\beta_i(\vec{\nu}_i)\, \nabla_s\, \varkappa_{\gamma,i} = \vec{0}. \tag{1.24c}$$

We note that (1.24b) prescribes an angle of $\alpha_i = 90^\circ$ between $[\gamma_i'(\vec{\nu}_i)]^\perp$ and the external boundary. This can be easily modified to

$$[\gamma_i'(\vec{\nu}_i)]^\perp \,.\, [\nabla F(\vec{x}_i(1))]^\perp = \cos\alpha_i, \tag{1.25}$$

in order to prescribe an arbitrary angle between $[\gamma_i'(\vec{\nu}_i)]^\perp$ and the external boundary $\partial\Omega$.

A network of curves with triple junctions, as e.g. previously described in Figure 4, moving under (anisotropic) motion by mean curvature can also be considered. Given the curves Γ_1, Γ_2, Γ_3, the normal velocity for each curve is then given by

$$\mathcal{V}_i = \beta_i(\vec{\nu}_i)\, \varkappa_{\gamma,i}, \qquad i = 1 \to 3, \tag{1.26}$$

as opposed to (1.20) for surface diffusion. In addition, the conditions (1.21a,b) have to hold at the triple junction points Λ_1 and Λ_2. That is, the chemical potential continuity condition, (1.21d), and the flux balance condition, (1.21c), in the surface diffusion case are dropped. As before, intersections of a curve with the external boundary $\partial\Omega$ can also be incorporated. Let $\partial\Omega$ be given by (1.23). Then, for the three given curves Γ_i, $i = 1 \to 3$, the conditions (1.21a,b) only need to hold at the triple junction $\Lambda = \vec{x}_i(0)$, $i = 1 \to 3$;

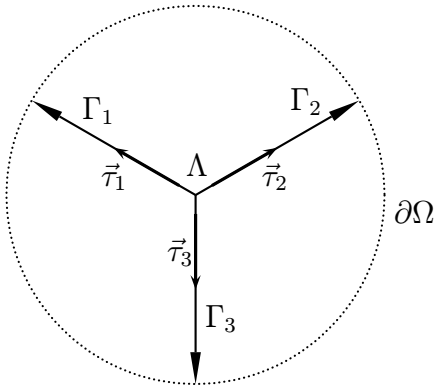

Figure 5: The second possible setup of $\Gamma = (\Gamma_1, \Gamma_2, \Gamma_3)$.

while (1.24a,b) hold at the boundary intersection points $\vec{x}_i(1)$, $i = 1 \to 3$. Once again, the flux balance condition, (1.24c), is dropped for mean curvature flow.

For parameterizations $\vec{x}_i \in \mathbb{R}^d$ of Γ_i, $i = 1 \to 3$, (1.26) can be written as a system of second order equations:

$$(\vec{x}_i)_t \,.\, \vec{\nu}_i = \beta_i(\vec{\nu}_i)\, \varkappa_{\gamma,i}, \qquad \varkappa_{\gamma,i}\, \vec{\nu}_i = [\gamma_i'(\vec{\nu}_i)]_s^\perp \,. \tag{1.27}$$

A variational formulation of (1.27), with the above stated conditions at triple junctions and boundary intersection points, will form the basis for our scheme that we present in Section 2. We remark that it is also possible to couple anisotropic mean curvature flow and anisotropic surface diffusion at triple junctions and it is straightforward to combine the methods of Barrett, Garcke, and Nürnberg (2006a), in which the isotropic case is studied, with the methods developed here to handle this situation.

The paper is organised as follows. In Section 2 we formulate a finite element approximation for (1.14a), (1.15) and derive stability bounds. Here we first introduce our approximation for the simpler cases of a closed curve, and then generalize that scheme to cover (1.20) and (1.21a–d) as well as (1.26) and (1.21a,b) in the case of a triple junction configuration as in Figure 4. We indicate on how to generalize the approach to a configuration as in Figure 5, as well as to an arbitrary setup of curves, triple junctions and external boundary intersections. In Section 3 we present numerous numerical computations.

2 Finite Element Approximation

2.1 Closed curves

We introduce the following finite element approximation. Let $J := \mathbb{R}/\mathbb{Z} = \cup_{j=1}^N J_j$, $N \geq 2$, be a decomposition of J into intervals given by the nodes q_j, $J_j = [q_{j-1}, q_j]$. Let $h_j = |J_j|$ and $h = \max_{j=1\to N} h_j$ be the maximal length of a grid element. Then the necessary finite

element spaces are defined as follows:

$$\underline{V}_0^h := \{\vec{\chi} \in C(J,\mathbb{R}^d) : \vec{\chi}|_{J_j} \text{ is linear } \forall\ j = 1 \to N\} =: [W_0^h]^d \subset H^1(J,\mathbb{R}^d),$$

where $W_0^h \subset H^1(J,\mathbb{R})$ is the space of scalar continuous (periodic) piecewise linear functions, with $\{\phi_l\}_{l=1}^N$ denoting the standard basis of W_0^h. Throughout this paper, we make use of the periodicity of J, i.e. $q_N \equiv q_0$, $q_{N+1} \equiv q_1$ and so on.

In addition, let $0 = t_0 < t_1 < \ldots < t_{M-1} < t_M = T$ be a partitioning of $[0,T]$ into possibly variable time steps $\tau_m := t_{m+1} - t_m$, $m = 0 \to M-1$. We set $\tau := \max_{m=0\to M-1} \tau_m$. Let $\vec{X}^m \in \underline{V}_0^h$ be an approximation to $\vec{x}(\cdot,t_m)$, and similarly $\kappa_\gamma^m \in W_0^h$ for $\varkappa_\gamma(\cdot,t_m)$.

For scalar, vector and matrix functions $u, v \in L^2(J,\mathbb{R})$, $L^2(J,\mathbb{R}^d)$ and $L^2(J,\mathbb{R}^{d\times d})$, respectively, we introduce the L^2 inner product $\langle\cdot,\cdot\rangle_m$ over the current polygonal curve Γ^m, which is described by the vector function $\vec{X}^m \in \underline{V}_0^h$, as follows

$$\langle u, v\rangle_m := \int_{\Gamma^m} u\,.\,v \,\mathrm{d}s = \int_J u\,.\,v\,|\vec{X}_\rho^m|\,\mathrm{d}\rho\,.$$

Here and throughout this paper, $\rho \in [0,1]$ is the parameterization variable. In addition, if u, v are piecewise continuous, with possible jumps at the nodes $\{q_j\}_{j=1}^N$, we define the mass lumped inner product $\langle\cdot,\cdot\rangle_m^h$ as

$$\langle u, v\rangle_m^h := \tfrac{1}{2}\sum_{j=1}^{N} |\vec{X}^m(q_j) - \vec{X}^m(q_{j-1})|\left[(u\,.\,v)(q_j^-) + (u\,.\,v)(q_{j-1}^+)\right], \tag{2.1}$$

where we define $u(q_j^\pm) := \lim\limits_{\varepsilon \searrow 0} u(q_j \pm \varepsilon)$. Furthermore, we note that

$$\nabla_s u\,.\,\nabla_s v = u_s\,.\,v_s = \frac{u_\rho\,.\,v_\rho}{|\vec{X}_\rho^m|^2} \qquad \text{and} \qquad \vec{\nu}^m = -[\vec{\tau}^m]^\perp = -\frac{(\vec{X}_\rho^m)^\perp}{|\vec{X}_\rho^m|}\,;$$

and in particular, we note also that for $\vec{u}, \vec{v} \in L^2(J,\mathbb{R}^d)$ and $\ell = 1 \to L$

$$(G^{(\ell)}\,\nabla_s\,\vec{u})\,.\,\nabla_s\,\vec{v} = (G^{(\ell)}\,\vec{u}_s\,[\vec{\tau}^m]^T)\,.\,(\vec{v}_s\,[\vec{\tau}^m]^T) = (G^{(\ell)}\,\vec{u}_s)\,.\,\vec{v}_s\,.$$

Hence, on recalling (1.3), (1.14a) and (1.15), we propose the following approximation to (1.10a): Find $\{\vec{X}^{m+1}, \kappa_\gamma^{m+1}\} \in \underline{V}_0^h \times W_0^h$ such that

$$\langle \frac{\vec{X}^{m+1} - \vec{X}^m}{\tau_m}, \chi\,\vec{\nu}^m\rangle_m^h - \langle \beta(\vec{\nu}^m)\,\kappa_\gamma^{m+1}, \chi\rangle_m^h = 0 \qquad \forall\ \chi \in W_0^h, \tag{2.2a}$$

$$\langle \kappa_\gamma^{m+1}\,\vec{\nu}^m, \vec{\eta}\rangle_m^h + \sum_{\ell=1}^{L} \langle [\gamma^{(\ell)}(\vec{\nu}^m)]^{-1}\,G^{(\ell)}\,\nabla_s\,[\vec{X}^{m+1}]^\perp, \nabla_s\,\vec{\eta}^\perp\rangle_m = 0 \qquad \forall\ \vec{\eta} \in \underline{V}_0^h, \tag{2.2b}$$

where, as noted above, the inner products $\langle\cdot,\cdot\rangle_m$, $\langle\cdot,\cdot\rangle_m^h$ as well as ∇_s depend on m. The corresponding approximation for motion by anisotropic surface diffusion, (1.10b), is given by: Find $\{\vec{X}^{m+1},\kappa_\gamma^{m+1}\}\in \underline{V}_0^h\times W_0^h$ such that

$$\langle\frac{\vec{X}^{m+1}-\vec{X}^m}{\tau_m},\chi\,\vec{\nu}^m\rangle_m^h-\langle\beta(\vec{\nu}^m)\,\nabla_s\,\kappa_\gamma^{m+1},\nabla_s\,\chi\rangle_m=0\qquad\forall\ \chi\in W_0^h \tag{2.3}$$

and (2.2b) hold. We note that (2.2a,b) and (2.3), (2.2b) for the isotropic surface energy $\gamma(\vec{p})=|\vec{p}|$ and the mobility $\beta\equiv 1$ collapse to the schemes considered in Barrett, Garcke, and Nürnberg (2006a) and Barrett, Garcke, and Nürnberg (2005), respectively.

In order to approximate (1.17), we adapt (2.2a) to

$$\langle\frac{\vec{X}^{m+1}-\vec{X}^m}{\tau_m},\chi\,\vec{\nu}^m\rangle_m^h-\langle\beta(\vec{\nu}^m)\,\kappa_\gamma^{m+1},\chi\rangle_m^h=-\frac{\langle\beta(\vec{\nu}^m)\,\kappa_\gamma^m,1\rangle_m^h}{\langle 1,1\rangle_m}\,\langle 1,\chi\rangle_m\qquad\forall\ \chi\in W_0^h. \tag{2.4}$$

REMARK. 2.1. *Nonlinear anisotropic mean curvature flows of the form* (1.11) *can be approximated by the scheme: Find* $\{\vec{X}^{m+1},\kappa_\gamma^{m+1}\}\in \underline{V}_0^h\times W_0^h$ *such that*

$$\langle\frac{\vec{X}^{m+1}-\vec{X}^m}{\tau_m},\chi\,\vec{\nu}^m\rangle_m^h-\langle\beta(\vec{\nu}^m)\,f(\kappa_\gamma^{m+1}),\chi\rangle_m^h=0\qquad\forall\ \chi\in W_0^h \tag{2.5}$$

and (2.2b) *hold. Under certain assumptions on* f *existence, uniqueness and stability can be shown for* (2.5) *and* (2.2b)*, see Barrett, Garcke, and Nürnberg (2006a) for the details in the isotropic case.*

REMARK. 2.2. *A possible approximation for* (1.12a) *and* (1.13)*, that can be used for an arbitrary anisotropy function* γ*, is the following. Find* $\{\vec{X}^{m+1},\ \kappa_\gamma^{m+1}\}\in \underline{V}_0^h\times W_0^h$ *such that*

$$\langle\frac{\vec{X}^{m+1}-\vec{X}^m}{\tau_m},\chi\,\vec{\nu}^m\rangle_m^h-\langle\beta(\vec{\nu}^m)\,\kappa_\gamma^{m+1},\chi\rangle_m^h=0\qquad\forall\ \chi\in W_0^h, \tag{2.6a}$$

$$\langle\kappa_\gamma^{m+1}\,\vec{\nu}^m,\vec{\eta}\rangle_m^h+\langle\gamma(\vec{\nu}^m)\,\nabla_s\,\vec{X}^{m+1},\nabla_s\,\vec{\eta}\rangle_m=\langle[\vec{\nu}^m\,[\gamma'(\vec{\nu}^m)]^T],\nabla_s\,\vec{\eta}\rangle_m\quad\forall\ \vec{\eta}\in\underline{V}_0^h. \tag{2.6b}$$

The system (2.6a,b) *uses a similar time discretization to the scheme studied in Clarenz, Dziuk, and Rumpf (2003). We note that as* $d=2$*, the right hand side value of* (2.6b) *is given by* $\int_{\Gamma^m}(\vec{\eta}_s\,.\,\vec{\nu}^m)\,(\gamma'(\vec{\nu}^m)\,.\,\vec{\tau}^m)\,\mathrm{d}s$*. We note that although in practice the approximation* (2.6a,b) *behaves well, it does not appear possible to prove a stability result similar to* Theorem 2.2*, below. Moreover, the corresponding scheme for anisotropic surface diffusion,* (2.3) *and* (2.6b)*, is unstable in practice, unless a very small time step size* τ *is used; and it usually eventually fails in practice due to the coalescence of mesh points. We observed a similar behaviour in practice for a scheme that treats the right hand side term in* (2.6b) *semi-implicitly.*

Before we can proceed to prove existence and uniqueness to (2.2a,b) and (2.3), (2.2b), we have to make the following very mild assumption.

($\mathcal{A}_0$) Let $|\vec{X}^m_\rho| > 0$ for almost all $\rho \in J$. For $j = 1 \to N$, let $\vec{\nu}^m_{j-\frac{1}{2}} := -\frac{(\vec{X}^m_\rho)^\perp}{|\vec{X}^m_\rho|}\,|_{J_j}$, and set

$$\begin{aligned}\vec{\omega}^m_j &:= \frac{|\vec{X}^m(q_j) - \vec{X}^m(q_{j-1})|\,\vec{\nu}^m_{j-\frac{1}{2}} + |\vec{X}^m(q_{j+1}) - \vec{X}^m(q_j)|\,\vec{\nu}^m_{j+\frac{1}{2}}}{|\vec{X}^m(q_j) - \vec{X}^m(q_{j-1})| + |\vec{X}^m(q_{j+1}) - \vec{X}^m(q_j)|} \\ &= \frac{-[\vec{X}^m(q_{j+1}) - \vec{X}^m(q_{j-1})]^\perp}{|\vec{X}^m(q_j) - \vec{X}^m(q_{j-1})| + |\vec{X}^m(q_{j+1}) - \vec{X}^m(q_j)|}\,. \end{aligned} \tag{2.7}$$

Then we further assume that $\dim \operatorname{span}\{\vec{\omega}^m_j\}_{j=1}^N = d = 2$.

REMARK. 2.3. *We note that one can interpret $\vec{\omega}^m_j$ as a weighted normal defined at the node $\vec{X}(q_j)$ of the curve Γ^m, where in general $|\vec{\omega}^m_j| < 1$. In addition, we note that ($\mathcal{A}_0$) is only violated in very rare occasions. For example, it always holds for curves without self intersections, see Barrett, Garcke, and Nürnberg (2005, Remark 2.2) for details.*

THEOREM. 2.1. *Let the assumption ($\mathcal{A}_0$) hold. Then there exists a unique solution $\{\vec{X}^{m+1}, \kappa^{m+1}\} \in \underline{V}^h_0 \times W^h_0$ to the systems* (2.2a,b) *and* (2.3), (2.2b).

Proof. As (2.2a,b) is linear, existence follows from uniqueness. To investigate the latter, we consider the system: Find $\{\vec{X}, \kappa_\gamma\} \in \underline{V}^h_0 \times W^h_0$ such that

$$\langle \vec{X}, \chi\,\vec{\nu}^m\rangle^h_m - \tau_m\,\langle \beta(\vec{\nu}^m)\,\kappa_\gamma, \chi\rangle^h_m = 0 \qquad \forall\ \chi \in W^h_0, \tag{2.8a}$$

$$\langle \kappa_\gamma\,\vec{\nu}^m, \vec{\eta}\rangle^h_m + \sum_{\ell=1}^{L} \langle [\gamma^{(\ell)}(\vec{\nu}^m)]^{-1}\,G^{(\ell)}\,\nabla_s\,\vec{X}^\perp, \nabla_s\,\vec{\eta}^\perp\rangle_m = 0 \qquad \forall\ \vec{\eta} \in \underline{V}^h_0. \tag{2.8b}$$

Choosing $\chi = \kappa_\gamma \in W^h_0$ in (2.8a) and $\vec{\eta} = \vec{X} \in \underline{V}^h_0$ in (2.8b) yields that

$$\sum_{\ell=1}^{L} \langle [\gamma^{(\ell)}(\vec{\nu}^m)]^{-1}\,G^{(\ell)}\,\nabla_s\,\vec{X}^\perp, \nabla_s\,\vec{X}^\perp\rangle_m + \tau_m\,\langle \beta(\vec{\nu}^m)\,\kappa_\gamma, \kappa_\gamma\rangle^h_m = 0\,. \tag{2.9}$$

It follows from (2.9), the positive definiteness of $G^{(\ell)}$, $\ell = 1 \to L$, and the positivity of β that $\kappa_\gamma \equiv 0$ and $\vec{X} \equiv \vec{X}^c \in \mathbb{R}^d$; and hence that

$$\langle \vec{X}^c, \chi\,\vec{\nu}^m\rangle^h_m = 0 \quad \forall\ \chi \in W^h_0. \tag{2.10}$$

Choosing $\chi = \phi_j$ in (2.10) yields that $\vec{X}^c\,.\,\vec{\omega}^m_j = 0$ for all $j = 1 \to N$. It follows from assumption ($\mathcal{A}_0$) that $\vec{X}^c = \vec{0}$. Hence we have shown that (2.2a,b) has a unique solution $\{\vec{X}^{m+1}, \kappa^{m+1}_\gamma\} \in \underline{V}^h_0 \times W^h_0$.

The corresponding proof for the system (2.3), (2.2b) is identical with only a small modification; see e.g. Barrett, Garcke, and Nürnberg (2005). ∎

Here, and throughout, let $\cdot_{(*)}$ denote an expression with or without the subscript $*$ and let $\vec{Id}_n \in (\mathbb{R}^{d\times d})^{n\times n}$ be the identity matrix, and similarly for $Id_n \in \mathbb{R}^{n\times n}$. We introduce

also the matrices $\vec{N}_0 \in (\mathbb{R}^d)^{N\times N}$, $M_{\beta,0}, A_{(\beta,)0} \in \mathbb{R}^{N\times N}$ and $\vec{A}_0 \in (\mathbb{R}^{d\times d})^{N\times N}$ with entries

$$[M_{\beta,0}]_{kl} := \langle \beta(\vec{\nu}^m)\,\phi_k, \phi_l\rangle_m^h, \quad [\vec{N}_0]_{kl} := \int_{\Gamma^m} \pi^h[\phi_k\,\phi_l]\,\vec{\nu}^m \,\mathrm{d}s, \quad [A_0]_{kl} := \langle \nabla_s\,\phi_k, \nabla_s\,\phi_l\rangle_m,$$
$$[A_{\beta,0}]_{kl} := \langle \beta(\vec{\nu}^m)\,\nabla_s\,\phi_k, \nabla_s\,\phi_l\rangle_m, \quad [\vec{A}_0]_{kl} := [A_0]_{kl} \sum_{\ell=1}^{L} [\gamma^{(\ell)}(\vec{\nu}^m)]^{-1}\, R(-\tfrac{\pi}{2})\, G^{(\ell)}\, R(\tfrac{\pi}{2})\,, \tag{2.11}$$

where we recall the definition of $R(\theta)$ in (1.7), and where $\pi^h : C(J,\mathbb{R}) \to W_0^h$ is the standard interpolation operator at the nodes $\{q_j\}_{j=1}^N$. We can then formulate (2.2a,b) as: Find $\{\delta\vec{X}^{m+1}, \kappa_\gamma^{m+1}\} \in (\mathbb{R}^d)^N \times \mathbb{R}^N$, such that

$$\begin{pmatrix} \tau_m\, M_{\beta,0} & -\vec{N}_0^T \\ \vec{N}_0 & \vec{A}_0 \end{pmatrix} \begin{pmatrix} \kappa^{m+1} \\ \delta\vec{X}^{m+1} \end{pmatrix} = \begin{pmatrix} 0 \\ -\vec{A}_0\,\vec{X}^m \end{pmatrix}, \tag{2.12}$$

where, with the obvious abuse of notation, $\delta\vec{X}^{m+1} = (\delta\vec{X}_1^{m+1}, \ldots, \delta\vec{X}_N^{m+1})^T$ and $\kappa_\gamma^{m+1} = (\kappa_1^{m+1}, \ldots, \kappa_N^{m+1})^T$ are the vectors of coefficients with respect to the standard basis of $\vec{X}^{m+1} - \vec{X}^m$ and κ_γ^{m+1}, respectively. We can transform (2.12) to

$$\kappa_\gamma^{m+1} = \tfrac{1}{\tau_m}\, M_{\beta,0}^{-1}\, \vec{N}_0^T\, \delta\vec{X}^{m+1}, \tag{2.13a}$$
$$(\vec{A}_0 + \tfrac{1}{\tau_m}\, \vec{N}_0\, M_{\beta,0}^{-1}\, \vec{N}_0^T)\, \delta\vec{X}^{m+1} = -\vec{A}_0\,\vec{X}^m. \tag{2.13b}$$

As (2.13b) is clearly symmetric and positive definite, there exists a unique solution to (2.13b). Moreover, the solution to (2.13a,b) uniquely solves (2.2a,b).

In order to adapt (2.13a,b) to the approximation (2.3), (2.2b) of motion by anisotropic surface diffusion, i.e. (2.12) with $M_{\beta,0}$ replaced by $A_{\beta,0}$, we need the following definitions; see Barrett, Garcke, and Nürnberg (2005) for their equivalents in the isotropic case. Let S_0 be the inverse of $A_{\beta,0}$ restricted on the subspace $(\ker A_{\beta,0})^\perp \equiv (\mathrm{span}\{1\})^\perp$, where $1 := (1,\ldots,1)^T \in \mathbb{R}^N$. Let $\vec{\Pi}_0$ be the orthogonal projection onto $\mathcal{R}_0^\perp := \{\vec{X} \in (\mathbb{R}^d)^N : \vec{X}^T\vec{N}_0 1 = 0\}$; that is, $\vec{\Pi}_0 := \vec{Id}_N - \frac{\vec{w}\vec{w}^T}{\vec{w}^T\vec{w}}$, where $\vec{w} := \vec{N}_0 1$. One can then employ a Schur complement approach to yield

$$\kappa_\gamma^{m+1} = \tfrac{1}{\tau_m}\, S_0\, \vec{N}_0^T\, \delta\vec{X}^{m+1}, \tag{2.14a}$$
$$\vec{\Pi}_0\,(\vec{A}_0 + \tfrac{1}{\tau_m}\, \vec{N}_0\, S_0\, \vec{N}_0^T)\, \vec{\Pi}_0\, \delta\vec{X}^{m+1} = -\vec{\Pi}_0\,\vec{A}_0\,\vec{X}^m. \tag{2.14b}$$

As (2.3), (2.2b) has a unique solution, it is easily established that there exists a unique solution to (2.14b). Moreover, the system (2.14b) is symmetric and positive definite on $\mathcal{R}_0^\perp$, see Barrett, Garcke, and Nürnberg (2005) for the relevant details.

Furthermore, we can establish that our schemes are unconditionally stable.

THEOREM. 2.2. *Let $\{\vec{X}^m, \kappa_\gamma^m\}_{m=1}^M$ be the solution of* (2.2a,b). *Then for $k = 1 \to M$ we have that*

$$|\Gamma^k|_\gamma + \sum_{m=0}^{k-1} \tau_m\, \langle \beta(\vec{\nu}^m)\,\kappa_\gamma^{m+1}, \kappa_\gamma^{m+1}\rangle_m^h \le |\Gamma^0|_\gamma\,, \tag{2.15a}$$

where we recall (1.1). *Similarly, the solution to* (2.3), (2.2b) *satisfies*

$$|\Gamma^k|_\gamma + \sum_{m=0}^{k-1} \tau_m \, \langle \beta(\vec{\nu}^m) \, \nabla_s \, \kappa_\gamma^{m+1}, \nabla_s \, \kappa_\gamma^{m+1} \rangle_m \leq |\Gamma^0|_\gamma \tag{2.15b}$$

for $k = 1 \to M$.

Proof. As the two proofs are almost identical, it is sufficient to show (2.15b). Choosing $\chi = \kappa_\gamma^{m+1} \in W_0^h$ in (2.3) and $\vec{\eta} = \frac{\vec{X}^{m+1} - \vec{X}^m}{\tau_m} \in \underline{V}_0^h$ in (2.2b) yields that

$$\sum_{\ell=1}^{L} \langle [\gamma^{(\ell)}(\vec{\nu}^m)]^{-1} \, G^{(\ell)} \, \nabla_s \, [\vec{X}^{m+1}]^\perp, \nabla_s \, (\vec{X}^{m+1} - \vec{X}^m)^\perp \rangle_m + \tau_m \, \langle \beta(\vec{\nu}^m) \, \nabla_s \, \kappa_\gamma^{m+1}, \nabla_s \, \kappa_\gamma^{m+1} \rangle_m = 0 \,. \tag{2.16}$$

We now analyse the first term in (2.16), similarly to the techniques used in Barrett, Garcke, and Nürnberg (2005), based on ideas in Dziuk (1999b) for the isostropic case. Let $\vec{h}_j^m := \vec{X}^m(q_j) - \vec{X}^m(q_{j-1})$. Then it holds for any $\ell \in \{1, \ldots, L\}$ that

$$\begin{aligned}
&\langle [\gamma^{(\ell)}(\vec{\nu}^m)]^{-1} \, G^{(\ell)} \, \nabla_s \, [\vec{X}^{m+1}]^\perp, \nabla_s \, (\vec{X}^{m+1} - \vec{X}^m)^\perp \rangle_m \\
&\qquad = \sum_{j=1}^{N} \left[\frac{[\vec{h}_j^{m+1}]^\perp \, . \, G^{(\ell)} \, (\, [\vec{h}_j^{m+1}]^\perp - [\vec{h}_j^m]^\perp \,)}{\gamma^{(\ell)}([\vec{h}_j^m]^\perp)} \right] \\
&\qquad = \sum_{j=1}^{N} \left[\frac{(\gamma^{(\ell)}([\vec{h}_j^{m+1}]^\perp) - \gamma^{(\ell)}([\vec{h}_j^m]^\perp))^2}{\gamma^{(\ell)}([\vec{h}_j^m]^\perp)} \right] \\
&\qquad\qquad + \sum_{j=1}^{N} \left[\frac{\gamma^{(\ell)}([\vec{h}_j^{m+1}]^\perp) \, \gamma^{(\ell)}([\vec{h}_j^m]^\perp) - [\vec{h}_j^{m+1}]^\perp \, . \, G^{(\ell)} \, [\vec{h}_j^m]^\perp}{\gamma^{(\ell)}([\vec{h}_j^m]^\perp)} \right] \\
&\qquad\qquad + \sum_{j=1}^{N} \left[\gamma^{(\ell)}([\vec{h}_j^{m+1}]^\perp) - \gamma^{(\ell)}([\vec{h}_j^m]^\perp) \right] \\
&\qquad \geq \sum_{j=1}^{N} \left[\gamma^{(\ell)}([\vec{h}_j^{m+1}]^\perp) - \gamma^{(\ell)}([\vec{h}_j^m]^\perp) \right] \\
&\qquad = \int_{\Gamma^{m+1}} \gamma^{(\ell)}(\vec{\nu}^{m+1}) \, \mathrm{d}s - \int_{\Gamma^m} \gamma^{(\ell)}(\vec{\nu}^m) \, \mathrm{d}s \,.
\end{aligned} \tag{2.17}$$

Summing (2.17) for $\ell = 1 \to L$ and combining with (2.16) yields that

$$|\Gamma^{m+1}|_\gamma - |\Gamma^m|_\gamma + \tau_m \, \langle \beta(\vec{\nu}^m) \, \nabla_s \, \kappa_\gamma^{m+1}, \nabla_s \, \kappa_\gamma^{m+1} \rangle_m \leq 0 \,. \tag{2.18}$$

Summing (2.18) for $m = 0 \to k-1$ yields the desired result (2.15b). ∎

We note that (2.15b) is a discrete analogue of (1.16). To our knowledge, this is the first stability result for a fully discrete direct approximation of (1.9a,b) or (1.10a,b).

REMARK. 2.4. *In Section 3, we will report on computations for our scheme* (2.2a,b)*, and compare our results with another scheme for anisotropic mean curvature flow. The scheme is based on the semi-discrete approximation from Dziuk (1999a), which for the anisotropy* (1.3) *and the natural analogue of our time discretization in* (2.2a,b) *can be written as: Find* $\vec{X}^{m+1} \in \underline{V}_0^h$ *such that*

$$\langle \beta(\vec{\nu}^m)^{-1}\, \frac{\vec{X}^{m+1}-\vec{X}^m}{\tau_m}, \vec{\eta}\rangle_m^h + \sum_{\ell=1}^{L} \langle [\gamma^{(\ell)}(\vec{\nu}^m)]^{-1}\, G^{(\ell)}\, \nabla_s\, [\vec{X}^{m+1}]^\perp, \nabla_s\, \vec{\eta}^\perp\rangle_m = 0 \quad \forall\ \vec{\eta} \in \underline{V}_0^h, \tag{2.19}$$

see also Deckelnick, Dziuk, and Elliott (2005a, p. 197). The system (2.19) *is a discretization of the variational formulation of*

$$\text{(a)} \quad [\beta)(\vec{\nu})]^{-1}\, \vec{x}_t = \varkappa_\gamma\, \vec{\nu} \qquad \textit{and} \qquad \text{(b)} \quad \varkappa_\gamma\, \vec{\nu} = [\gamma'(\vec{\nu})]_s^\perp; \tag{2.20}$$

as opposed to our scheme (2.2a,b)*, which is a discretization of* (1.12a) *and* (2.20b)*. We note that* (2.2a,b) *with* $\beta \equiv 1$ *can be rewritten as: Find* $\vec{X}^{m+1} \in \underline{V}_0^h$ *such that*

$$\langle \frac{\vec{X}^{m+1}-\vec{X}^m}{\tau_m}\,.\,\vec{\omega}^m, \vec{\eta}\,.\,\vec{\omega}^m\rangle_m^h + \sum_{\ell=1}^{L} \langle [\gamma^{(\ell)}(\vec{\nu}^m)]^{-1}\, G^{(\ell)}\, \nabla_s\, [\vec{X}^{m+1}]^\perp, \nabla_s\, \vec{\eta}^\perp\rangle_m = 0 \quad \forall\ \vec{\eta} \in \underline{V}_0^h\,; \tag{2.21}$$

which clearly highlights the key difference between the two schemes. The scheme (2.19) *changes the approximation of* $\vec{x}$ *predominantly in the normal direction, recall* (2.20a)*; whereas the scheme* (2.21) *proposed in this paper also induces tangential changes. This is a crucial difference. We note that for the semi-discrete version of* (2.19) *and for an (admissable) class of anisotropies, which in particular includes* (1.3)*, stability and error bounds have been derived in Dziuk (1999a). Of course, it is simple matter to adapt the proof of* (2.15a) *to prove an analogous stability result for* (2.19)*.*

REMARK. 2.5. *It is worthwhile to consider a continuous in time semidiscrete version of our schemes. Here we replace e.g.* (2.3)*,* (2.2b) *by*

$$\langle \vec{X}_t, \chi\, \vec{\nu}^h\rangle^h - \langle \beta(\vec{\nu}^m)\, \nabla_s\, \kappa_\gamma, \nabla_s\, \chi\rangle = 0 \qquad \forall\, \chi \in W_0^h, \tag{2.22a}$$

$$\langle \kappa_\gamma\, \vec{\nu}^h, \vec{\eta}\rangle^h + \sum_{\ell=1}^{L} \langle [\gamma^\ell(\vec{\nu}^h)]^{-1}\, G^{(\ell)}\, \nabla_s\, \vec{X}^\perp, \nabla_s\, \vec{\eta}^\perp\rangle = 0 \qquad \forall\, \vec{\eta} \in \underline{V}_0^h; \tag{2.22b}$$

where we always integrate over the current curve Γ^h*, described by* $\vec{X}$*, and so* $\vec{\nu}^h = -\frac{(\vec{X}_\rho)^\perp}{|\vec{X}_\rho|}$ *and* $\langle\cdot,\cdot\rangle$*,* $\langle\cdot,\cdot\rangle^h$ *are the same as* $\langle\cdot,\cdot\rangle_m$*,* $\langle\cdot,\cdot\rangle_m^h$ *with* Γ^m *and* $\vec{X}^m$ *replaced by* Γ^h *and* $\vec{X}$*, respectively. It is now straightforward to show that* (2.22a,b) *conserves the enclosed area,* $a^h(t)$*, exactly; since on choosing* $\chi = 1$ *in* (2.22a) *and taking into account* (2.1) *yields that*

$$0 = \langle \vec{X}_t, \vec{\nu}^h\rangle^h = \int_{\Gamma^h} \vec{X}_t\,.\,\vec{\nu}^h\, \mathrm{d}s = \frac{d}{dt}\, a^h(t). \tag{2.23}$$

To our knowledge, no other direct approximation of (1.10b) *in the literature satisfies this property.*

Furthermore the scheme (2.22a,b), *and its analogue for the approximation* (2.2a,b), *will always equidistribute the vertices along* Γ^h *with respect to a non-trivial weighting function. To see this, choose* $\vec{\eta} = (\vec{\omega}_j^h)^\perp \, \phi_j \in \underline{V}_0^h$ *in* (2.22b), *where* $\vec{\omega}_j^h$ *is the* Γ^h *analogue of* $\vec{\omega}_j^m$, *which yields, on recalling* (1.3), (2.1), (2.7) *and* (1.2), *that for* $j = 1 \to N$

$$
\begin{aligned}
&\Big[\gamma'(\vec{X}_{j+1} - \vec{X}_j) - \gamma'(\vec{X}_j - \vec{X}_{j-1})\Big] . (\vec{X}_{j+1} - \vec{X}_{j-1}) = 0 \quad \Rightarrow \\
&\sum_{\ell=1}^{L} [\, \gamma^{(\ell)}(\vec{X}_{j+1} - \vec{X}_j) - \gamma^{(\ell)}(\vec{X}_j - \vec{X}_{j-1}) \,] \, [1 - \frac{(\vec{X}_{j+1} - \vec{X}_j) \, . \, G^{(\ell)} \, (\vec{X}_j - \vec{X}_{j-1})}{\gamma^{(\ell)}(\vec{X}_{j+1} - \vec{X}_j) \, \gamma^{(\ell)}(\vec{X}_j - \vec{X}_{j-1})} \,] = 0 \\
&\Rightarrow \;\; \textit{either} \; \sum_{\ell=1}^{L} \lambda_j^{(\ell)} \, \gamma^{(\ell)}(\vec{X}_{j+1} - \vec{X}_j) = \sum_{\ell=1}^{L} \lambda_j^{(\ell)} \, \gamma^{(\ell)}(\vec{X}_j - \vec{X}_{j-1}) \\
&\qquad \textit{or} \;\; [\vec{X}_{j+1} - \vec{X}_j] \parallel [\vec{X}_j - \vec{X}_{j-1}] \, ,
\end{aligned}
\tag{2.24}
$$

where $\lambda_j^{(\ell)} := 1 - \frac{(\vec{X}_{j+1} - \vec{X}_j) \, . \, G^{(\ell)} \, (\vec{X}_j - \vec{X}_{j-1})}{\gamma^{(\ell)}(\vec{X}_{j+1} - \vec{X}_j) \, \gamma^{(\ell)}(\vec{X}_j - \vec{X}_{j-1})} \in (0, 1]$, $\ell = 1 \to L$. *In the special case* $L = 1$ *we note, provided intervals are not locally parallel, that* (2.24) *gives equidistribution with respect to* γ*; which in the isotropic case yields an equidistribution of the vertices, as discussed in Barrett, Garcke, and Nürnberg (2005). For* $L \geq 2$, *however, this is no longer true. Moreover, it does not appear possible to prove the analogues of* (2.23) *and* (2.24) *for the fully discrete scheme* (2.2a,b). *However, in practice we observe that the enclosed area is approximately preserved, and that the area loss tends to zero as* $\tau \to 0$. *In practice we see also that for* $L = 1$ *the vertices are moved tangentially so that they will eventually be equidistributed with respect to* γ, *i.e.* $\gamma(\vec{X}_j - \vec{X}_{j-1})$, $j = 1 \to N$, *is constant. Furthermore, even for* $L \geq 2$ *the induced tangential movement means that no heuristical redistribution of vertices is necessary in practice. See Section 3 for details.*

2.1.1 Intermediate evolution laws

In this subsection we consider the intermediate motion (1.19). We introduce the following approximation to (1.19). Find $\{\vec{X}^{m+1}, Y^{m+1}, \kappa_\gamma^{m+1}\} \in \underline{V}_0^h \times [W_0^h]^2$ such that

$$
\langle \frac{\vec{X}^{m+1} - \vec{X}^m}{\tau_m}, \chi \, \vec{\nu}^m \rangle_m^h - \langle \beta(\vec{\nu}^m) \, \nabla_s \, Y^{m+1}, \nabla_s \, \chi \rangle_m = 0 \qquad \forall \; \chi \in W_0^h, \tag{2.25a}
$$

$$
\tfrac{1}{\xi} \, \langle \beta(\vec{\nu}^m) \, \nabla_s \, Y^{m+1}, \nabla_s \, \chi \rangle_m + \tfrac{1}{\alpha} \, \langle \beta(\vec{\nu}^m) \, Y^{m+1}, \chi \rangle_m^h - \langle \beta(\vec{\nu}^m) \, \kappa_\gamma^{m+1}, \chi \rangle_m^h = 0 \qquad \forall \; \chi \in W_0^h \tag{2.25b}
$$

and (2.2b) hold.

THEOREM. 2.3. *Let the assumption* $(\mathcal{A}_0)$ *hold. Then there exists a unique solution* $\{\vec{X}^{m+1}, Y^{m+1}, \kappa_\gamma^{m+1}\} \in \underline{V}_0^h \times [W_0^h]^2$ *to the system* (2.25a,b), (2.2b). *Moreover, we have*

that

$$|\Gamma^k|_\gamma + \tfrac{1}{\alpha}\sum_{m=0}^{k-1} \tau_m \,\langle \beta(\vec{\nu}^m)\,\nabla_s\, Y^{m+1}, \nabla_s\, Y^{m+1}\rangle_m + \xi \sum_{m=0}^{k-1} \tau_m \,|[\beta(\vec{\nu}^m)]^{\frac{1}{2}}\,(\kappa_\gamma^{m+1} - \tfrac{1}{\alpha}\, Y^{m+1})|^2_{m,h} \\ \leq |\Gamma^0|_\gamma \tag{2.26}$$

for $k = 1 \to M$, *where* $|\cdot|^2_{m,h} := \langle \cdot, \cdot \rangle^h_m$.

Proof. The existence and uniqueness proof is a straightforward adaption of the proof to Theorem 2.1, and for the isotropic case can be found in Barrett, Garcke, and Nürnberg (2006a, Theorem 2.2). The proof of the stability result (2.26) in the isotropic case can also be found there. It is easily extended to the anisotropic case on noting (2.17). ∎

On recalling the definitions (2.11), we can reformulate (2.25a,b), (2.2b) as: Find $\{\delta\vec{X}^{m+1}, Y^{m+1}\,\kappa_\gamma^{m+1}\} \in (\mathbb{R}^d)^N \times [\mathbb{R}^N]^2$, such that

$$\begin{pmatrix} 0 & \tau_m\, A_{\beta,0} & -\vec{N}_0^T \\ -M_{\beta,0} & \frac{1}{\xi}\, A_{\beta,0} + \frac{1}{\alpha}\, M_{\beta,0} & 0 \\ \vec{N}_0 & 0 & \vec{A}_0 \end{pmatrix} \begin{pmatrix} \kappa_\gamma^{m+1} \\ Y^{m+1} \\ \delta\vec{X}^{m+1} \end{pmatrix} = \begin{pmatrix} 0 \\ 0 \\ -\vec{A}_0\,\vec{X}^m \end{pmatrix}, \tag{2.27}$$

where, with the obvious abuse of notation, $\delta\vec{X}^{m+1}$, Y^{m+1} and κ_γ^{m+1} are the vectors of coefficients with respect to the standard basis of $\vec{X}^{m+1} - \vec{X}^m$, Y^{m+1} and κ_γ^{m+1}, respectively. We can employ a Schur complement approach to transform (2.27) to

$$\vec{\Pi}_0\,(\vec{A}_0 + \tfrac{1}{\tau_m}\vec{N}_0\,[\tfrac{1}{\alpha}\, S_0 + \tfrac{1}{\xi}\, M_{\beta,0}^{-1}]\,\vec{N}_0^T)\,\vec{\Pi}_0\,\delta\vec{X}^{m+1} = -\vec{\Pi}_0\,\vec{A}_0\,\vec{X}^m, \tag{2.28}$$

see Barrett, Garcke, and Nürnberg (2006a) for details. Again, it is easily established that there exists a unique solution to (2.28). Moreover, the system (2.28) is symmetric and positive definite on $\mathcal{R}_0^\perp$.

2.2 Triple junctions

In this section, we consider the case where a network of curves meeting at triple junction points moves under anisotropic motion by mean curvature or under anisotropic surface diffusion. Here the curves can meet at triple junction points or can intersect the external boundary $\partial\Omega$. For ease of exposition, from now on we consider the two cases of three curves $(\Gamma_1, \Gamma_2, \Gamma_3)$ with given anisotropies $\gamma := (\gamma_1, \gamma_2, \gamma_3)$, where $\gamma_i = \sum_{\ell=1}^{L_i} \gamma_i^{(\ell)}$, $i = 1 \to 3$, is of the form (1.3), and mobilities $\beta := (\beta_1, \beta_2, \beta_3)$ meeting either at two triple junction points Λ_1 and Λ_2, as in Figure 4; or meeting at a single triple junction point Λ_1 and each intersecting the external boundary $\partial\Omega$, as in Figure 5. In particular, we note the stated choices of the direction of the unit tangents. We have outlined in the papers Barrett, Garcke, and Nürnberg (2005, Remark 2.5) and Barrett, Garcke, and Nürnberg (2006a, Remark 2.7) how the ideas presented for these cases can be carried over to an arbitrary

setup of curves in the isotropic case. With minor modifications, the same holds true for the anisotropic flows considered in this paper.

We begin with the first setup. The main idea for the necessary trial ($\equiv$ test) spaces is to make sure, that the conditions (1.21a–d) hold either essentially or weakly at the triple junctions. Here we will enforce conditions (1.21a,d) explicitly through the trial space, whereas conditions (1.21b,c) will be enforced weakly, similarly to a Neumann boundary condition for a standard second order elliptic PDE.

Let $I := [0,1]$ be the unit interval and let $I = \cup_{j=1}^{N_i} I_j^i$, $i = 1 \to 3$, be decompositions of I into intervals $I_j^i = [q_{j-1}^i, q_j^i]$ based on the nodes $\{q_j^i\}_{j=0}^{N_i}$, $N_i \geq 2$. Let $h_j^i = |I_j^i|$ and $h = \max_{i=1\to 3} \max_{j=1\to N_i} h_j^i$ be the maximal length of a grid element. Let

$$\begin{aligned} \underline{V} &:= \{(\vec{\chi}_1, \vec{\chi}_2, \vec{\chi}_3) \in [C(I, \mathbb{R}^d)]^3 : \vec{\chi}_1 = \vec{\chi}_2 = \vec{\chi}_3 \text{ on } \partial I\}, \\ W &:= \{(\chi_1, \chi_2, \chi_3) \in [C(I, \mathbb{R})]^3 : \chi_1 + \chi_2 + \chi_3 = 0 \ \text{ on } \partial I\} \end{aligned}$$

and $W_{\mathcal{M}} := \{(\chi_1, \chi_2, \chi_3) \in [C(I, \mathbb{R})]^3\}$. The appropriate finite element spaces are then defined by

$$\underline{V}^h := \{(\vec{\chi}_1, \vec{\chi}_2, \vec{\chi}_3) \in \underline{V} : \vec{\chi}_i|_{I_j^i} \text{ is linear } \forall\ j = 1 \to N_i,\ i = 1 \to 3\} \subset \underline{V} \tag{2.29}$$

and similarly for the spaces of scalar functions $W^h \subset W$ and $W_{\mathcal{M}}^h \subset W_{\mathcal{M}}$.

Recall the time partitioning $\{\tau_m\}_{m=0}^{M-1}$ and let $\vec{X}^m \in \underline{V}^h$ be an approximation to $\vec{x}(\cdot, t_m) \equiv (\vec{x}_1, \vec{x}_2, \vec{x}_3)(\cdot, t_m)$. We introduce the L^2 inner product $\langle \cdot, \cdot \rangle_m$ and the mass lumped inner product $\langle \cdot, \cdot \rangle_m^h$ over the current surface $\Gamma^m := (\Gamma_1^m, \Gamma_2^m, \Gamma_3^m)$, which is described by the vector function $\vec{X}^m \in \underline{V}^h$, for scalar, vector and matrix functions $u, v \in [L^2(I, \mathbb{R})]^3$, $[L^2(I, \mathbb{R}^d)]^3$ and $[L^2(I, \mathbb{R}^{d\times d})]^3$, as follows:

$$\begin{aligned} \langle u, v \rangle_m &:= \int_{\Gamma^m} u \,.\, v \, \mathrm{d}s := \sum_{i=1}^{3} \int_I u_i \,.\, v_i \, |(\vec{X}_i^m)_\rho| \, \mathrm{d}\rho, \\ \langle u, v \rangle_m^h &:= \sum_{i=1}^{3} \tfrac{1}{2} \sum_{j=1}^{N_i} |\vec{X}_i^m(q_j^i) - \vec{X}_i^m(q_{j-1}^i)| \left[(u_i \,.\, v_i)([q_j^i]^-) + (u_i \,.\, v_i)([q_{j-1}^i]^+) \right]. \end{aligned} \tag{2.30}$$

In addition, we note that

$$(\nabla_s u \,.\, \nabla_s v)|_{\Gamma_i^m} = \frac{(u_i)_\rho \,.\, (v_i)_\rho}{|(\vec{X}_i^m)_\rho|^2}, \qquad \vec{\nu}^m|_{\Gamma_i^m} = -\frac{[(\vec{X}_i^m)_\rho]^\perp}{|(\vec{X}_i^m)_\rho|}, \qquad i = 1 \to 3.$$

We then propose the following approximation to (1.22) and (1.21a–d): Find $\{\vec{X}^{m+1}, \kappa_\gamma^{m+1}\} \in \underline{V}^h \times W^h$ such that

$$\langle \frac{\vec{X}^{m+1} - \vec{X}^m}{\tau_m}, \chi \, \vec{\nu}^m \rangle_m^h - \langle \beta(\vec{\nu}^m) \, \nabla_s \, \kappa_\gamma^{m+1}, \nabla_s \, \chi \rangle_m = 0 \qquad \forall\ \chi \in W^h, \tag{2.31a}$$

$$\langle \kappa_\gamma^{m+1} \, \vec{\nu}^m, \vec{\eta} \rangle_m^h + \langle \sum_\ell [\gamma^{(\ell)}(\vec{\nu}^m)]^{-1} \, G^{(\ell)} \, \nabla_s \, [\vec{X}^{m+1}]^\perp, \nabla_s \, \vec{\eta}^\perp \rangle_m = 0 \qquad \forall\ \vec{\eta} \in \underline{V}^h, \tag{2.31b}$$

where we have used the obvious notation

$$\langle \sum_{\ell} [\gamma^{(\ell)}(\vec{\nu}^m)]^{-1}\, G^{(\ell)}\, \nabla_s\, [\vec{X}^{m+1}]^{\perp}, \nabla_s\, \vec{\eta}^{\perp} \rangle_m :=$$

$$\sum_{i=1}^{3} \int_{\Gamma_i^m} \sum_{\ell=1}^{L_i} [\gamma_i^{(\ell)}(\vec{\nu}_i^m)]^{-1}\, G_i^{(\ell)}\, \nabla_s\, [\vec{X}_i^{m+1}]^{\perp}\, .\, \nabla_s\, \vec{\eta}_i^{\perp}\, \mathrm{d}s.$$

Observe that (2.31a,b) was derived from (1.22) using integration by parts and the definition of the spaces W^h and $\underline{V}^h$. On noting that $(\nabla_s\, \vec{X}^{m+1})\,|_{\Gamma_i^m}$ approximates $\vec{\tau}_i^m$, $i = 1 \to 3$, we see that (2.31b) weakly approximates (1.21b) at the triple junction points Λ_1 and Λ_2, while (2.31a) weakly approximates (1.21c).

The corresponding scheme to approximate (1.27) and (1.21a,b) is then given by: Find $\{\vec{X}^{m+1}, \kappa_\gamma^{m+1}\} \in \underline{V}^h \times W_{\mathcal{M}}^h$ such that

$$\langle \frac{\vec{X}^{m+1} - \vec{X}^m}{\tau_m}, \chi\, \vec{\nu}^m \rangle_m^h - \langle \beta(\vec{\nu}^m)\, \kappa_\gamma^{m+1}, \chi \rangle_m = 0 \qquad \forall\ \chi \in W_{\mathcal{M}}^h, \quad (2.32a)$$

$$\langle \kappa_\gamma^{m+1}\, \vec{\nu}^m, \vec{\eta} \rangle_m^h + \langle \sum_{\ell} [\gamma^{(\ell)}(\vec{\nu}^m)]^{-1}\, G^{(\ell)}\, \nabla_s\, [\vec{X}^{m+1}]^{\perp}, \nabla_s\, \vec{\eta}^{\perp} \rangle_m = 0 \qquad \forall\ \vec{\eta} \in \underline{V}^h. \quad (2.32b)$$

Before we can proceed to prove existence and uniqueness to (2.31a,b) and (2.32a,b), we have to make the following very mild assumption.

($\mathcal{A}$) Let $|(\vec{X}_i^m)_\rho| > 0$ for almost all $\rho \in I$, $i = 1 \to 3$. Let $\vec{\nu}_{i,j-\frac{1}{2}}^m := -\frac{[(\vec{X}_i^m)_\rho]^{\perp}}{|(\vec{X}_i^m)_\rho|}\,|_{I_j^i}$, $j = 1 \to N_i$ and set $\vec{\omega}_{i,j}^m := \frac{|\vec{X}_i^m(q_j^i) - \vec{X}_i^m(q_{j-1}^i)|\, \vec{\nu}_{i,j-\frac{1}{2}}^m + |\vec{X}_i^m(q_{j+1}^i) - \vec{X}_i^m(q_j^i)|\, \vec{\nu}_{i,j+\frac{1}{2}}^m}{|\vec{X}_i^m(q_j^i) - \vec{X}_i^m(q_{j-1}^i)| + |\vec{X}_i^m(q_{j+1}^i) - \vec{X}_i^m(q_j^i)|}$, $j = 1 \to N_i - 1$, $i = 1 \to 3$. Then we assume further that for each $i = 1 \to 3$ there exists a $j \in \{1, \ldots, N_i - 1\}$ such that $\vec{\omega}_{i,j}^m \neq \vec{0}$. Moreover, we require that $\dim \mathrm{span}\{\{\vec{\omega}_{i,j}^m\}_{j=1}^{N_i-1}\}_{i=1}^3 = d = 2$.

The assumption ($\mathcal{A}$) basically assures that none of the the curves Γ_i^m, $i = 1 \to 3$, is a "zig zagging" connection between the two triple junctions points Λ_1 and Λ_2, see Barrett, Garcke, and Nürnberg (2005) for details.

THEOREM. 2.4. *Let the assumption* ($\mathcal{A}$) *hold. Then there exist unique solutions* $\{\vec{X}^{m+1}, \kappa_\gamma^{m+1}\} \in \underline{V}^h \times W^h$ *to the system* (2.31a,b) *and* $\{\vec{X}^{m+1}, \kappa_\gamma^{m+1}\} \in \underline{V}^h \times W_{\mathcal{M}}^h$ *to the system* (2.32a,b).

Proof. The proof is a direct analogue of the proof for Theorem 2.1. See also Barrett, Garcke, and Nürnberg (2005, Theorem 2.2) for details in the isotropic case. ∎

REMARK. 2.6. *Similarly to* (2.22a,b), *in a time continuous semidiscrete version of our scheme* (2.31a,b) *we obtain exact area conservation, as testing for example with* $\chi = (-1, 1, 0) \in W^h$ *in the analogue of* (2.31a) *leads to*

$$0 = \int_{\Gamma_2^h} [\vec{X}_2]_t\, .\, \vec{\nu}^h\, \mathrm{d}s - \int_{\Gamma_1^h} [\vec{X}_1]_t\, .\, \vec{\nu}^h\, \mathrm{d}s = \frac{d}{dt}\, a_3^h(t),$$

where $a_3^h(t)$ is the area enclosed by Γ_1^h and Γ_2^h. Moreover, the condition (2.24) *now yields that vertices will be equidistributed (with respect to some non-trivial weighting function) on all curve segments of Γ_i^h, that are not locally parallel. Although we are unable to prove such results for the fully discrete scheme* (2.31a,b)*, the change relative to the initial area never exceeded* 1% *in our simulations. In addition, we observed the equidistribution property for* (2.31a,b) *and* (2.32a,b) *in practice.*

Furthermore, we can establish that our scheme is unconditionally stable.

THEOREM. 2.5. *Let $\{\vec{X}^m, \kappa_\gamma^m\}_{m=1}^M$ be the solution of* (2.31a,b)*. Then for $k = 1 \to M$ we have that*

$$|\Gamma^k|_\gamma + \sum_{m=0}^{k-1} \tau_m \left\langle \beta(\vec{\nu}^m)\, \nabla_s\, \kappa_\gamma^{m+1}, \nabla_s\, \kappa_\gamma^{m+1} \right\rangle_m \leq |\Gamma^0|_\gamma\,,$$

where $|\Gamma^k|_\gamma := \int_{\Gamma^k} \gamma(\vec{\nu}^k)\, \mathrm{d}s \equiv \sum_{i=1}^3 |\Gamma_i^k|_\gamma$ on recalling the definition (2.30)*. Correspondingly, we have for the solution to* (2.32a,b) *that*

$$|\Gamma^k|_\gamma + \sum_{m=0}^{k-1} \tau_m \left\langle \beta(\vec{\nu}^m)\, \kappa_\gamma^{m+1}, \kappa_\gamma^{m+1} \right\rangle_m^h \leq |\Gamma^0|_\gamma\,,$$

for $k = 1 \to M$.

Proof. The proof is a direct analogue of the proof for Theorem 2.2. See also Barrett, Garcke, and Nürnberg (2005, Theorem 2.3) for details in the isotropic case. ∎

2.2.1 Schur complement approach

We now generalize the Schur complement approach in Barrett, Garcke, and Nürnberg (2005) to the anisotropic situation considered in this paper. Let $N := \sum_{i=1}^3 (N_i + 1)$. We define the orthogonal projections

$$K : \mathbb{R}^N \to \mathbb{X} := \{(z_1, z_2, z_3) \in \mathbb{R}^N : \sum_{i=1}^3 [z_i]_0 = \sum_{i=1}^3 [z_i]_{N_i} = 0\}$$

and $\vec{P} : (\mathbb{R}^d)^N \to \underline{\mathbb{X}} := \{(\vec{z}_1, \vec{z}_2, \vec{z}_3) \in (\mathbb{R}^d)^N : [\vec{z}_1]_0 = [\vec{z}_2]_0 = [\vec{z}_3]_0, [\vec{z}_1]_{N_1} = [\vec{z}_2]_{N_2} = [\vec{z}_3]_{N_3}\}$ onto the Euclidean spaces associated with W^h and $\underline{V}^h$, respectively.

In order to give a matrix formulation for (2.31a,b) we introduce the matrices $\vec{N}^i \in (\mathbb{R}^d)^{(N_i+1)\times(N_i+1)}$, $\vec{A}^i \in (\mathbb{R}^{d\times d})^{(N_i+1)\times(N_i+1)}$ and $M_\beta^i, A_{(\beta)}^i \in \mathbb{R}^{(N_i+1)\times(N_i+1)}$, $i = 1 \to 3$,

defined by

$$\vec{N}^i_{kl} := \int_{\Gamma^m_i} \pi^h_i[\phi^i_k\,\phi^i_l]\,\vec{\nu}^m\,\mathrm{d}s, \quad [M^i_\beta]_{kl} := \int_{\Gamma^m_i} \beta(\vec{\nu}^m)\,\pi^h_i[\phi^i_k\,\phi^i_l]\,\mathrm{d}s,$$
$$[A^i_\beta]_{kl} := \int_{\Gamma^m_i} \beta(\vec{\nu}^m)\,\nabla_s\,\phi^i_k\,.\,\nabla_s\,\phi^i_l\,\mathrm{d}s, \quad A^i_{kl} := \int_{\Gamma^m_i} \nabla_s\,\phi^i_k\,.\,\nabla_s\,\phi^i_l\,\mathrm{d}s,$$
$$\vec{A}^i_{kl} := A^i_{kl}\,\sum_{\ell=1}^{L_i}[\gamma^{(\ell)}_i(\vec{\nu}^m_i)]^{-1}\,R(-\tfrac{\pi}{2})\,G^{(\ell)}_i\,R(\tfrac{\pi}{2})\,,$$

where $\{\phi^i_l\}_{l=0}^{N_i}$ is the standard basis of $S^h_i := \{\chi \in C(I,\mathbb{R}) : \chi\,|_{I^i_j}$ is linear $\forall\ j = 1 \to N_i\}$ and $\pi^h_i : C(I,\mathbb{R}) \to S^h_i$ is the standard interpolation operator at the nodes $\{q^i_j\}_{j=0}^{N_i}$. Then, on introducing the matrices

$$A_\beta := \begin{pmatrix} A^1_\beta & 0 & 0 \\ 0 & A^2_\beta & 0 \\ 0 & 0 & A^3_\beta \end{pmatrix},\ \vec{A} := \begin{pmatrix} \vec{A}^1 & 0 & 0 \\ 0 & \vec{A}^2 & 0 \\ 0 & 0 & \vec{A}^3 \end{pmatrix},\ \vec{N} := \begin{pmatrix} \vec{N}^1 & 0 & 0 \\ 0 & \vec{N}^2 & 0 \\ 0 & 0 & \vec{N}^3 \end{pmatrix},$$

and similarly $M_\beta := \mathrm{diag}\,(M^1_\beta, M^2_\beta, M^3_\beta)$, where $A_\beta, M_\beta : \mathbb{R}^N \to \mathbb{R}^N$, $\vec{A} : (\mathbb{R}^d)^N \to (\mathbb{R}^d)^N$ and $\vec{N} : \mathbb{R}^N \to (\mathbb{R}^d)^N$, the system of equations (2.31a,b) can be written as: Find $\{\delta\vec{X}^{m+1}, \kappa^{m+1}_\gamma\} \in \underline{\mathbb{X}} \times \mathbb{X}$ such that

$$\begin{pmatrix} \tau_m\,K A_\beta K & -K\vec{N}^T\vec{P} \\ \vec{P}\vec{N}K & \vec{P}\vec{A}\vec{P} \end{pmatrix} \begin{pmatrix} \kappa^{m+1}_\gamma \\ \delta\vec{X}^{m+1} \end{pmatrix} = \begin{pmatrix} 0 \\ -\vec{P}\vec{A}\vec{P}\,\vec{X}^m \end{pmatrix}. \tag{2.33}$$

Here, with the obvious abuse of notation similarly to (2.12), $\kappa^{m+1}_\gamma = (\kappa^{m+1}_1, \kappa^{m+1}_2, \kappa^{m+1}_3)^T$ with $\kappa^{m+1}_i = ([\kappa^{m+1}_i]_0, \ldots, [\kappa^{m+1}_i]_{N_i})$, $i = 1 \to 3$, and $\delta\vec{X}^{m+1} = (\delta\vec{X}^{m+1}_1, \delta\vec{X}^{m+1}_2, \delta\vec{X}^{m+1}_3)^T$ with $\delta\vec{X}^{m+1}_i = ([\delta\vec{X}^{m+1}_i]_0, \ldots, [\delta\vec{X}^{m+1}_i]_{N_i})$, $i = 1 \to 3$, are the vectors of coefficients with respect to the standard basis $\{\{\phi^i_l\}_{l=0}^{N_i}\}_{i=1}^3$ of κ^{m+1}_γ and $\vec{X}^{m+1} - \vec{X}^m$ in (2.31a,b), respectively.

We note that the kernel of $KA_\beta K$ is the direct sum of $\ker K$ and the space $E = \ker A_\beta \cap \mathbb{X}$ spanned by the two null vectors $e_1 := (1^1, -1^2, 0) \in \mathbb{X}$ and $e_2 := (0, 1^2, -1^3) \in \mathbb{X}$ of $KA_\beta K$, where $1^i := (1, \ldots, 1)^T \in \mathbb{R}^{N_i+1}$, $i = 1 \to 3$. I.e. $\ker KA_\beta K = \ker K \oplus \mathrm{span}\{e_i : i = 1 \to 2\} \equiv \mathbb{X}^\perp \oplus \mathrm{span}\{e_i : i = 1 \to 2\}$. Introducing the inverse S of $KA_\beta K$ restricted on the set $(\ker KA_\beta K)^\perp \subset \mathbb{R}^N$, i.e. $S\,KA_\beta K\,v = KA_\beta K\,S\,v = v$ for all $v \in (\ker KA_\beta K)^\perp$, and defining the space $\mathcal{R} := \mathrm{span}\,\{\vec{P}\vec{N}K\,e_i : i = 1 \to 2\} \equiv \{\vec{P}\vec{N}K\,v : v \in \ker KA_\beta K\} \subset \underline{\mathbb{X}}$; we note from the first equation of (2.33) that $\delta\vec{X}^{m+1} \in \mathcal{T} := \mathcal{R}^\perp \cap \underline{\mathbb{X}}$ and hence that $K\vec{N}^T\vec{P}\,\delta\vec{X}^{m+1} \in (\ker KA_\beta K)^\perp$. Therefore, we can employ a Schur complement approach

in order to transform (2.33) to

$$\kappa_\gamma^{m+1} = \tfrac{1}{\tau_m}\, S\, K \vec{N}^T \vec{P}\, \delta\vec{X}^{m+1} + \sum_{i=1}^{2} \mu_i\, e_i, \tag{2.34a}$$

$$(\vec{P}\vec{A}\vec{P} + \tfrac{1}{\tau_m}\, \vec{P}\vec{N} K\, S\, K \vec{N}^T \vec{P})\, \delta\vec{X}^{m+1} = -\vec{P}\vec{A}\vec{P}\, \vec{X}^m - \sum_{i=1}^{2} \mu_i\, \vec{P}\vec{N} K\, e_i, \quad \delta\vec{X}^{m+1} \in \mathcal{T}; \tag{2.34b}$$

where in (2.34a) we have used the fact that $\kappa_\gamma^{m+1} \in \mathbb{X}$ and where $\mu_i \in \mathbb{R}$ are unknown. Let $\vec{\Pi} : (\mathbb{R}^d)^N \to \mathcal{R}^\perp$ be the orthogonal projection onto $\mathcal{R}^\perp$. Then, on noting that $\delta\vec{X}^{m+1} \in \mathcal{R}^\perp$, (2.34b) can be simplified to

$$\vec{\Pi}\, \vec{P}\, (\vec{A} + \tfrac{1}{\tau_m}\, \vec{N} K\, S\, K \vec{N}^T)\, \vec{P}\, \vec{\Pi}\, \delta\vec{X}^{m+1} = -\vec{\Pi}\, \vec{P}\vec{A}\vec{P}\, \vec{X}^m. \tag{2.35}$$

REMARK. 2.7. *A possible definition for the projection* $\vec{\Pi}$ *is* $\vec{\Pi} := \vec{Id}_N - \vec{Q}\, \vec{Q}^T$, *where* $\operatorname{im} \vec{Q} = \mathcal{R}$ *and* $\vec{Q}^T \vec{Q} = Id_2$. *I.e. the columns of* $\vec{Q} \in (\mathbb{R}^d)^{N\times 2}$ *are an orthonormal basis of the subspace* $\mathcal{R} \subset (\mathbb{R}^d)^N$ *spanned by* $\vec{P}\vec{N}Ke_i \equiv \vec{P}\vec{N}\, e_i$, *where* $e_i \in \mathbb{X}$, $i = 1 \to 2$, *are the above mentioned null vectors of* $KA_\beta K$. *We note that the definitions of* $\vec{P}$ *and* $\vec{N}$ *yield that* $\dim \mathcal{R} = 2$. *Hence* $\vec{\Pi}$ *is the orthogonal projection from* $(\mathbb{R}^d)^N$ *onto* $(\operatorname{im} \vec{Q})^\perp \equiv \mathcal{R}^\perp$.

REMARK. 2.8. *The definition of* $\vec{\Pi}$ *can easily be adapted to a situation with* K_B *bubbles/areas. Now the subspace* E *of the kernel of* $KA_\beta K$ *has dimension* K_B, *and a possible basis consists of vectors that each "describe an admissible orientation of the boundary of a bubble" in terms of the given* K_C *curves. E.g. if* $K_B = 3$ *and one area is enclosed by curves* $1, 2, 4$ *and curve* 2 *is parameterized in the opposite direction to curves* 1 *and* 4, *then the corresponding eigenvector would be* $(1^1, -1^2, 0, 1^4, 0, 0)$. *See the appendix in Barrett, Garcke, and Nürnberg (2005) for more details.*

THEOREM. 2.6. *Let* $\{\delta\vec{X}^{m+1}, \kappa_\gamma^{m+1}\} \in \underline{\mathbb{X}} \times \mathbb{X}$ *be the unique solution to* (2.33). *Then* $\delta\vec{X}^{m+1}$ *uniquely solves* (2.35). *Moreover, the operator in* (2.35) *is symmetric positive definite.*

Proof. The proof is a straightforward adaption of the proof in Barrett, Garcke, and Nürnberg (2005, Theorem 2.4). □

Similarly, a simple extension of the isotropic case in Barrett, Garcke, and Nürnberg (2006a) leads to the following Schur complement system for our anisotropic approximation (2.32a,b):

$$\kappa_\gamma^{m+1} = \tfrac{1}{\tau_m}\, M_\beta^{-1} \vec{N}^T \vec{P}\, \delta\vec{X}^{m+1}, \tag{2.36a}$$

$$\vec{P}\, (\vec{A} + \tfrac{1}{\tau_m}\, \vec{N}\, M_\beta^{-1}\, \vec{N}^T)\, \vec{P}\, \delta\vec{X}^{m+1} = -\vec{P}\vec{A}\vec{P}\, \vec{X}^m. \tag{2.36b}$$

2.2.2 Boundary intersections

We now recall the necessary function spaces introduced in Barrett, Garcke, and Nürnberg (2006a) in order to adapt our approximation to the setup as depicted in Figure 5. For a given $\vec{X}^m \in [C(I,\mathbb{R}^d)]^3$, let

$$\underline{V}_\partial(\vec{X}^m) := \{(\vec{\chi}_1,\vec{\chi}_2,\vec{\chi}_3) \in [C(I,\mathbb{R}^d)]^3 : \vec{\chi}_1(0) = \vec{\chi}_2(0) = \vec{\chi}_3(0) \quad \text{and} \\ \vec{\chi}_i(1)\,.\,\nabla F(\vec{X}_i^m(1)) = 0 \quad \forall\ i = 1 \to 3\}$$

and

$$W_\partial := \{(\chi_1,\chi_2,\chi_3) \in [C(I,\mathbb{R})]^3 : \chi_1(0) + \chi_2(0) + \chi_3(0) = 0\}.$$

The finite element spaces $\underline{V}_\partial^h(\vec{X}^m)$ and W_∂^h are then defined accordingly, similarly to (2.29). Moreover, the system (2.31a,b) is then adapted to: Find $\{\delta\vec{X}^{m+1}, \kappa_\gamma^{m+1}\} \in \underline{V}_\partial^h(\vec{X}^m) \times W_\partial^h$, where $\vec{X}^{m+1} := \vec{X}^m + \delta\vec{X}^{m+1}$, such that

$$\langle \frac{\delta\vec{X}^{m+1}}{\tau_m}, \chi\,\vec{\nu}^m\rangle_m^h - \langle \beta(\vec{\nu}^m)\,\nabla_s\,\kappa_\gamma^{m+1}, \nabla_s\,\chi\rangle_m^h = 0 \qquad \forall\ \chi \in W_\partial^h, \quad (2.37a)$$

$$\langle \kappa_\gamma^{m+1}\,\vec{\nu}^m, \vec{\eta}\rangle_m^h + \langle \sum_\ell [\gamma^{(\ell)}(\vec{\nu}^m)]^{-1}\,G^{(\ell)}\,\nabla_s\,[\vec{X}^{m+1}]^\perp, \nabla_s\,\vec{\eta}^\perp\rangle_m = 0 \qquad \forall\ \vec{\eta} \in \underline{V}_\partial^h(\vec{X}^m). \quad (2.37b)$$

We note that the constraint $\delta\vec{X}^{m+1} \in \underline{V}_\partial^h(\vec{X}^m)$ weakly enforces (1.24a), as it is a linearized approximation of these constraints. In particular, for curved boundaries the equations $F(\vec{X}_i^{m+1}(1)) = 0$, $i = 1 \to 3$, are only approximately satisfied, see Barrett, Garcke, and Nürnberg (2006a) for details.

In order to incorporate variable boundary contact angles as in (1.25), we add the term

$$\sum_{i=1}^3 \frac{[\nabla F(\vec{X}_i^m(1))]^\perp}{|\nabla F(\vec{X}_i^m(1))|}\,.\,\vec{\eta}_i(1)\,\cos\alpha_i$$

to the right hand side of (2.37b).

On defining the orthogonal projections $K_\partial : \mathbb{R}^N \to \mathbb{X}_\partial := \{(z_1,z_2,z_3) \in \mathbb{R}^N : \sum_{i=1}^3 [z_i]_0 = 0\}$ and $\vec{P}_\partial : (\mathbb{R}^d)^N \to \underline{\mathbb{X}}_\partial := \{(\vec{z}_1,\vec{z}_2,\vec{z}_3) \in (\mathbb{R}^d)^N : [\vec{z}_1]_0 = [\vec{z}_2]_0 = [\vec{z}_3]_0$ and $[\vec{z}_i]_{N_i}\,.\,\nabla F([\vec{X}_i^m]_{N_i}) = 0 \quad \forall\ i = 1 \to 3\}$ onto the Euclidean spaces associated with W_∂^h and $\underline{V}_\partial^h(\vec{X}^m)$, we can apply a Schur complement approach to yield

$$\vec{\Pi}_\partial\,\vec{P}_\partial\,(\vec{A} + \tfrac{1}{\tau_m}\,\vec{N}K_\partial\,S_\partial\,K_\partial\vec{N}^T)\,\vec{P}_\partial\,\vec{\Pi}_\partial\,\delta\vec{X}^{m+1} = -\vec{\Pi}_\partial\,\vec{P}_\partial\vec{A}\,\vec{X}^m, \quad (2.38)$$

where S_∂ is the inverse of $K_\partial A_\beta K_\partial$ on the space $(\ker K_\partial A_\beta K_\partial)^\perp$ and $\vec{\Pi}_\partial$ is the orthogonal projection from $\mathbb{R}^N$ onto $\mathcal{R}_\partial^\perp$ with $\mathcal{R}_\partial := \vec{P}_\partial\vec{N}K_\partial\,(\ker K_\partial A_\beta K_\partial)$. Again we refer to Barrett, Garcke, and Nürnberg (2006a) for the relevant details.

Similarly, the approximation (2.32a,b) can be adapted to the setup in Figure 5 as follows: Find $\{\delta\vec{X}^{m+1}, \kappa_\gamma^{m+1}\} \in \underline{V}_\partial^h(\vec{X}^m) \times W_{\mathcal{M}}^h$, such that (2.32a) and (2.37b) hold. The corresponding Schur complement approach then yields

$$\vec{P}_\partial \, (\vec{A} + \tfrac{1}{\tau_m} \, \vec{N} \, M_\beta^{-1} \, \vec{N}^T) \, \vec{P}_\partial \, \delta\vec{X}^{m+1} = -\vec{P}_\partial \vec{A} \, \vec{X}^m. \tag{2.39}$$

3 Results

The Schur complement approaches (2.13b), (2.14b), (2.35), (2.36b), (2.38) and (2.39) can be easily solved with a conjugate gradient solver, see Barrett, Garcke, and Nürnberg (2005) for details.

As the anisotropic evolution laws considered in this section can lead to a very non-uniform distribution of mesh points, it is essential to employ a suitable preconditioner for the above mentioned systems. In practice, the following diagonal preconditioner $\vec{G}_0 \in [\mathbb{R}^{d\times d}]^{N\times N}$ with diagonal entries

$$[\vec{G}_0]_{ii} = \left[[\vec{A}_0]_{ii} + \tfrac{1}{\tau_m} \, [M_{\beta,0}]_{ii}^{-1} \begin{pmatrix} ([\vec{N}_0]_{ii} \cdot \vec{e}_1)^2 & 0 \\ 0 & ([\vec{N}_0]_{ii} \cdot \vec{e}_2)^2 \end{pmatrix} \right]^{-1}, \tag{3.1}$$

where $\vec{e}_i$, $i = 1 \to d$, are the standard basis vectors in $\mathbb{R}^d$, worked very well for the system (2.13b). Naturally, the definition (3.1) can easily be adapted to all of the other Schur complement systems. For instance, for the system (2.14b) we used the preconditioner $\vec{\Pi}_0 \, \vec{H}_0 \, \vec{\Pi}_0$, where $\vec{H}_0 \in [\mathbb{R}^{d\times d}]^{N\times N}$ is obtained from (3.1) by replacing $[M_{\beta,0}]_{ii}$ with $[A_{\beta,0}]_{ii}$, while a suitable preconditioner for the system (2.35) is given by

$$\vec{\Pi} \, \vec{P} \vec{H} \vec{P} \, \vec{\Pi} \in [\mathbb{R}^{d\times d}]^{N\times N}, \tag{3.2}$$

where $\vec{H} \in [\mathbb{R}^{d\times d}]^{N\times N}$ is the obvious curve network analogue of the closed curve operator $\vec{H}_0$, i.e. its block entry $\vec{H}^i \in [\mathbb{R}^{d\times d}]^{(N_i+1)\times(N_i+1)}$ corresponding to Γ_i^m is diagonal and given by

$$[\vec{H}^i]_{kk} = \left[[\vec{A}^i]_{kk} + \tfrac{1}{\tau_m} \, [A_\beta^i]_{kk}^{-1} \begin{pmatrix} ([\vec{N}^i]_{kk} \cdot \vec{e}_1)^2 & 0 \\ 0 & ([\vec{N}^i]_{kk} \cdot \vec{e}_2)^2 \end{pmatrix} \right]^{-1}.$$

Note that for the computations reported on in this section the preconditioned conjugate gradient solver was up to 12 times faster than the standard conjugate gradient solver.

Throughout this section we use uniform time steps $\tau_m = \tau$, $m = 0 \to M-1$. For later purposes, we define

$$\vec{X}(t) := \tfrac{t-t_{m-1}}{\tau} \, \vec{X}^m + \tfrac{t_m - t}{\tau} \, \vec{X}^{m-1} \qquad t \in [t_{m-1}, t_m] \quad m \geq 1.$$

Unless otherwise stated, we use a constant mobility $\beta \equiv 1$ and for the curve network computations prescribe the same anisotropy $\gamma_i = \gamma_0$ and the same mobility $\beta_i \equiv 1$ on all of the curves.

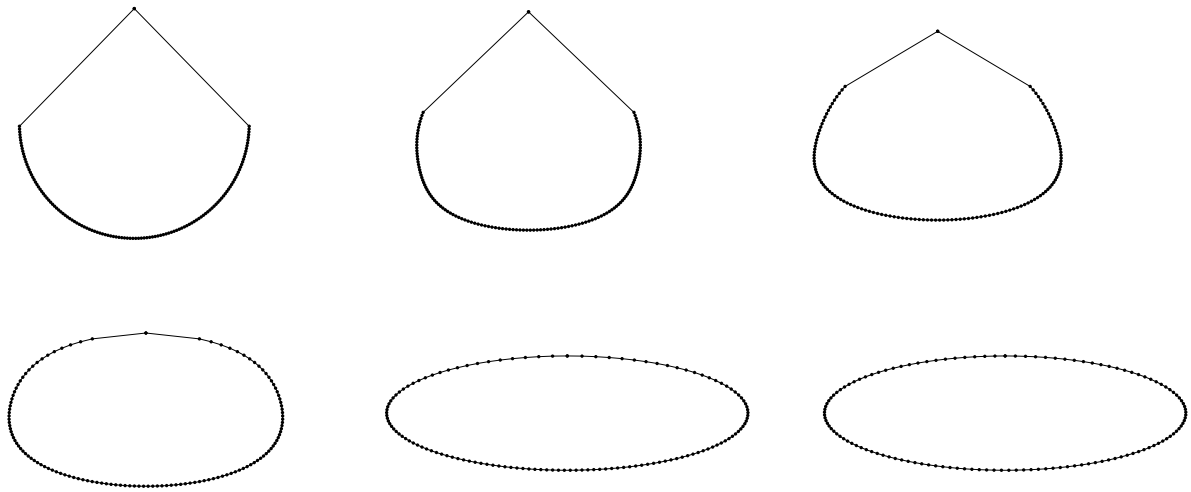

Figure 6: A plot of $\vec{X}(t)$ at times $t = 0,\ 0.01,\ 0.05,\ 0.1,\ 1,\ T = 4$.

3.1 Closed curves

3.1.1 Anisotropic surface diffusion

In our first experiment, we demonstrate the ability of our schemes to tangentially redistribute the mesh points. To this end, we use as an initial curve a parameterization of a semi-circle with radius 1 and a single additional node on the periphery of the circle. The results for our approximation (2.3), (2.2b), i.e. for motion by anisotropic surface diffusion, can be seen in Figure 6. Here we chose the anisotropy (1.7) with $L = 1$, $\theta_1 = 0$ and $\varepsilon_1^2 = 0.1$, and used the discretization parameters $N = 128$, $\tau = 10^{-3}$ and $T = 4$. We now investigate the ratio $r_\gamma := \max_{j=1\to N} \gamma([\vec{X}^m(q_j) - \vec{X}^m(q_{j-1})]^\perp) / \min_{j=1\to N} \gamma([\vec{X}^m(q_j) - \vec{X}^m(q_{j-1})]^\perp)$, over time. A plot of r_γ can be seen in Figure 7. The last plot in that figure shows the weighted length $|\Gamma|_\gamma$ of the computed curve over time. One can clearly see that although the Wulff shape (an ellipse) is reached very quickly (at around time $t = 0.6$), in the remaining time the vertices are continually moved tangentially, which results in a further decrease in the ratio r_γ, which approaches the optimal value 1. The evolution of a unit circle to the elliptic Wulff shape of the anisotropy (1.7) with $L = 1$, $\theta_1 = 0$ and $\varepsilon_1^2 = 0.01$ can be seen in Figure 8. We note that the domain enclosed by the curve is at times concave during the evolution. The discretization parameters were as before, except $T = 2$. The relative area loss for this experiment was 0.6%.

Next, we show an experiment for anisotropic surface diffusion, where the anisotropy is given by the regularized l^1 norm (1.4), or equivalently (1.7) with $L = 2$, $\varepsilon_\ell \equiv \varepsilon$ and $(\theta_1, \theta_2) = (0, \frac{\pi}{2})$. We varied the parameter $\varepsilon = 10^{-k}$, $k = 1 \to 3$; see Figure 9, where we show the steady state solutions. We can clearly see that the tangential movement of mesh points results in a higher density of vertices at the corners of the Wulff shape. The discretization parameters for the computations were $N = 100$, $\tau = 10^{-3}$ and $T = 1$.

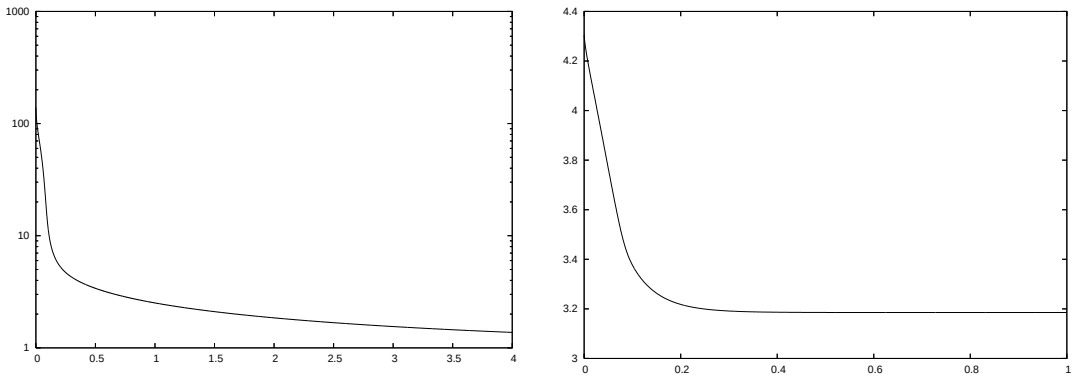

Figure 7: A plot of $\log r_\gamma$ over $[0, T]$. The second plot shows the weighted length $|\Gamma(t)|_\gamma$ for $t \in [0, 1]$.

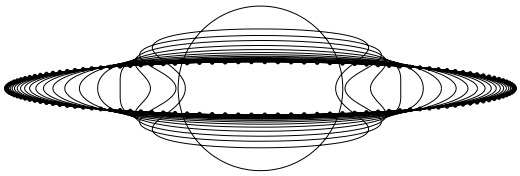

Figure 8: $\vec{X}(t)$ at times $t = 0,\ 0.1, \ldots, T = 2$.

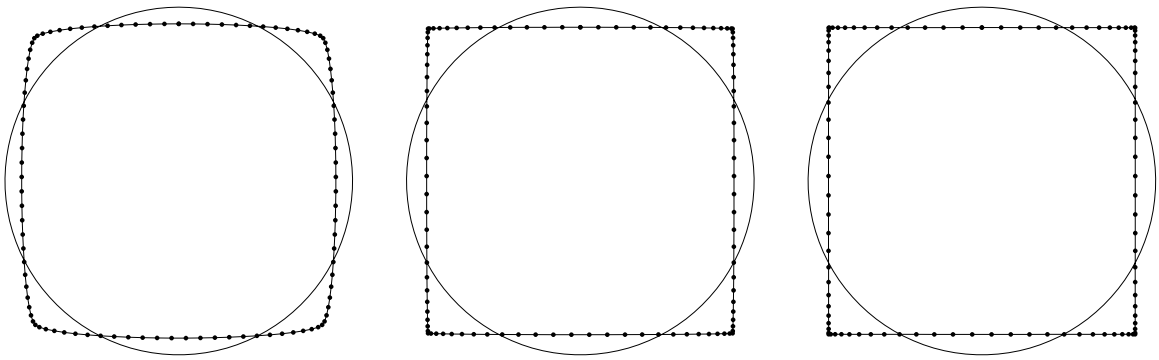

Figure 9: A plot of $\vec{X}(t)$ at times $t = 0,\ T = 1$ for the regularized l^1 norm (1.4) with $\varepsilon = 10^{-k}$, $k = 1 \to 3$.

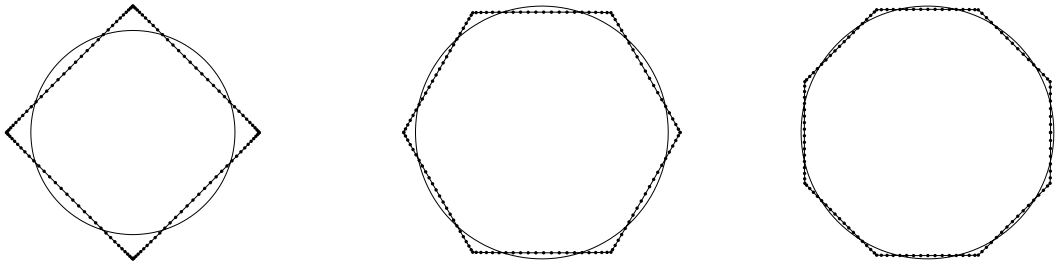

Figure 10: $\vec{X}(t)$ at times $t = 0,\ T = 1$.

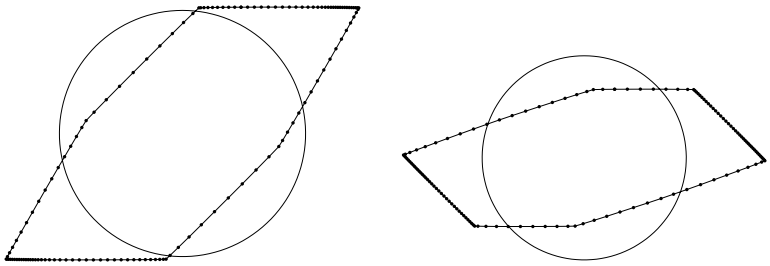

Figure 11: $\vec{X}(t)$ at times $t = 0,\ T = 1$.

An experiment for the anisotropy (1.7) with $\varepsilon_\ell^2 \equiv 10^{-4}$ and $(\theta_1, \ldots, \theta_L) = (\frac{\pi}{4}, \frac{3\pi}{4})$, $(0, \frac{\pi}{3}, \frac{2\pi}{3})$ or $(0, \frac{\pi}{4}, \frac{\pi}{2}, \frac{3\pi}{4})$ can be seen in Figure 10. The discretization parameters were $N = 128$, $\tau = 10^{-3}$ and $T = 1$. The relative area losses for this experiment were 0.79%, 0.26% and 0.08%, respectively. Similarly, experiments for the anisotropies with only a 2-fold symmetric Frank diagram in Figure 1 can be seen in Figure 11. Here we took (1.7) with $\varepsilon_\ell^2 \equiv 10^{-4}$ and $(\theta_1, \ldots, \theta_L) = (0, \frac{\pi}{4}, \frac{\pi}{3})$ or $(0, \frac{\pi}{10}, \frac{\pi}{9}, \frac{3\pi}{4})$ and used the same discretization parameters as before.

3.1.2 Anisotropic mean curvature flow

In this subsection we consider our approximation (2.2a,b) for motion by anisotropic mean curvature flow. In Figure 12 we show how the unit circle moves under anisotropic mean curvature, with γ given by (1.7) with $\varepsilon_\ell^2 \equiv 10^{-4}$ and $(\theta_1, \ldots, \theta_L) = (\frac{\pi}{4}, \frac{3\pi}{4})$ or $(0, \frac{\pi}{3}, \frac{2\pi}{3})$. The discretization parameters were $N = 128$, $\tau = 10^{-3}$ with $T = 0.35$ and $T = 0.25$, respectively.

We now repeat the last two experiments for the anisotropic mobility $\beta = \gamma$ in (2.2a). It was shown by Soner (1993) that then an exact solution to (1.10a) is given by

$$\Gamma(t) = \{\vec{q} \in \mathbb{R}^d : \gamma^*(\vec{q}) = \sqrt{1 - 2\,t}\}, \tag{3.1}$$

i.e. shrinking boundaries of Wulff shapes. See Figure 13 for the results, where we used the same discretization parameters as before, except $T = 0.38$ and $T = 0.14$, respectively.

The next experiment is for the anisotropy (1.7) with $L = 1$, $\theta_1 = 0$ and $\varepsilon_1 = 0.5$. The

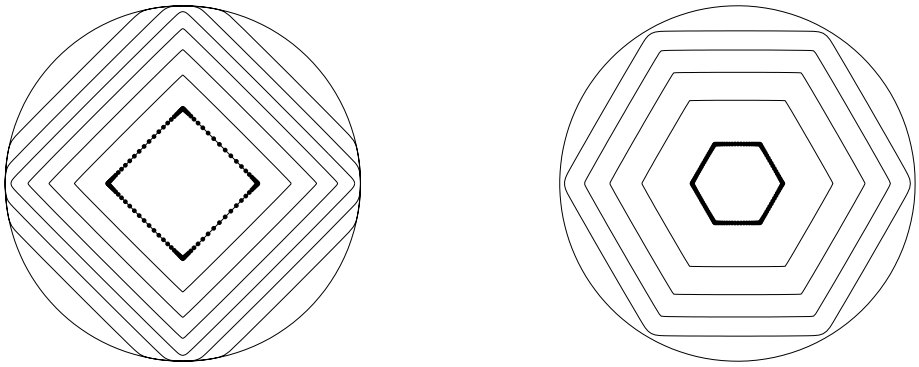

Figure 12: $\vec{X}(t)$ at times $t = 0,\ 0.05, \ldots, T$ with $T = 0.35$ (left) and $T = 0.25$ (right).

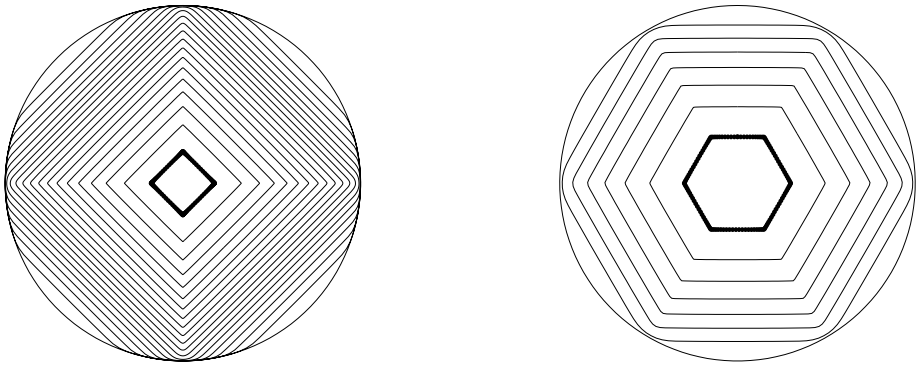

Figure 13: $\vec{X}(t)$ at times $t = 0,\ 0.02, \ldots, T$ with $T = 0.38$ (left) and $T = 0.14$ (right).

parameters were chosen as follows. $N = 128$, $\tau = 10^{-3}$, $T = 0.6$ and the initial curve is a unit circle. In order to highlight one difference between our approximation (2.2a,b) and the scheme (2.19), we plot for each of them the ratio r_γ over time. The evolution of our scheme (2.21) can be seen in Figure 14. Plots of the ratio r_γ for the two schemes can be seen in Figure 15. One can clearly see that the ratio increases for scheme (2.19), while the tangential movement of vertices induced by our scheme, as discussed in Remark 2.5, results in a decrease of the ratio r_γ, which approaches the optimal value 1.

Using (3.1) we now perform a convergence test for our approximation (2.2a,b) with $\beta = \gamma$. An exact solution to (1.10a) with $\beta = \gamma$ defined by (1.7) with $L = 1$, $\theta_1 = 0$, $\varepsilon_1 = \varepsilon$, on noting (1.6) and (3.1), is given by

$$\vec{x}(\rho, t) = (1 - 2\,t)^{\frac{1}{2}}\,(\cos g(\rho), \varepsilon\,\sin g(\rho))^T, \quad t \in [0, \overline{T}), \quad \overline{T} = 0.5; \tag{3.2}$$

where $g(\rho) = 2\pi\rho + 0.1\,\sin(2\pi\rho)$ in order to make the initial distribution of nodes non-uniform. For $\varepsilon = 0.5$ and $\varepsilon = 0.1$ we report on the error $\|\vec{X} - \vec{x}\|_{L^\infty}$ between $\vec{X}$ and the true solution (3.2) in Table 1. Here $\|\vec{X} - \vec{x}\|_{L^\infty} := \max_{m=1\to M} \|\vec{X}(t_m) - \vec{x}(\cdot, t_m)\|_{L^\infty}$, where $\|\vec{X}(t_m) - \vec{x}(\cdot, t_m)\|_{L^\infty} := \max_{j=1\to N} \min_{\rho\in J} |\vec{X}^m(q_j) - \vec{x}(\rho, t_m)|$, is computed by employing a Newton method. We used $\tau = 0.5\,h^2$ and either $T = \frac{1}{2}\,\overline{T}$ or $T = \overline{T} - \tau$. We note that the experiments indicate that the convergence rate for the error away from the

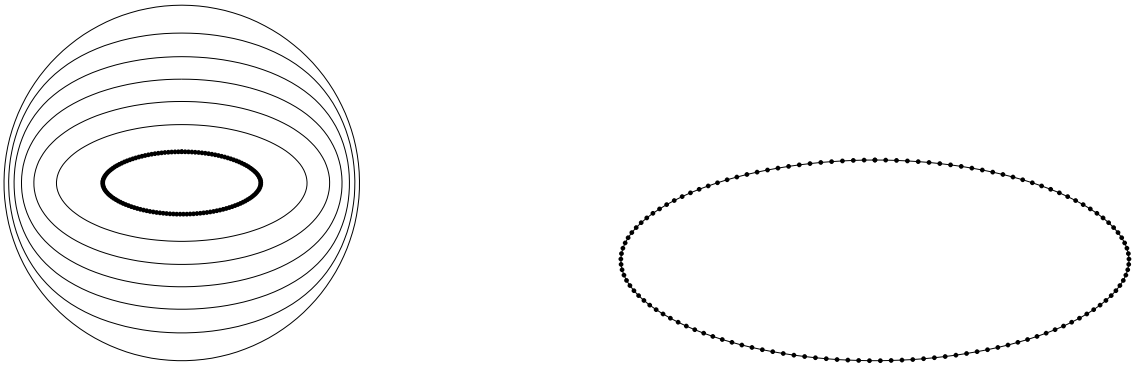

Figure 14: A plot of $\vec{X}(t)$ at times $t = 0,\ 0.1, \ldots, T = 0.6$ and at time $t = T$ (scaled).

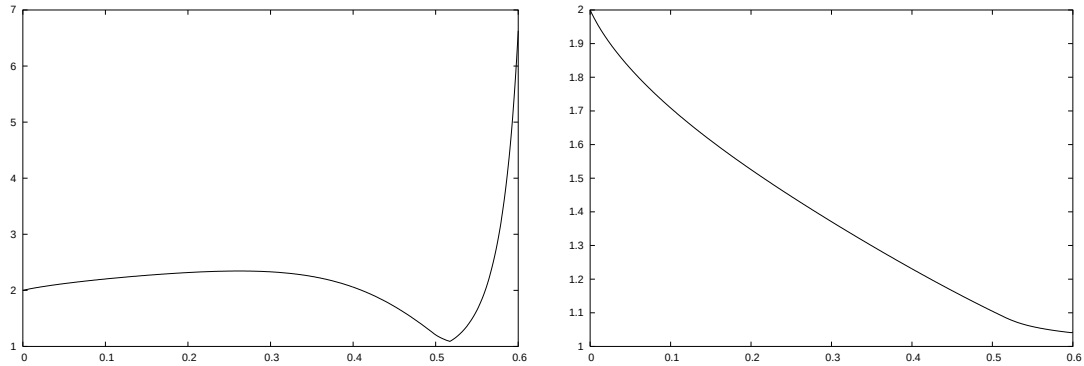

Figure 15: A plot of the ratio r_γ for the two schemes (2.19), left, and (2.21), right.

	$\varepsilon = 0.5$		$\varepsilon = 0.1$	
N	$T = \frac{1}{2}\overline{T}$	$T = \overline{T} - \tau$	$T = \frac{1}{2}\overline{T}$	$T = \overline{T} - \tau$
16	3.0459e-02	1.1445e-01	2.9858e-02	1.1417e-01
32	1.0179e-02	1.1089e-01	9.7928e-03	1.1037e-01
64	2.6967e-03	7.8884e-02	2.5734e-03	7.8814e-02
128	6.8419e-04	5.0824e-02	6.7007e-04	5.0815e-02
256	1.7180e-04	3.0543e-02	1.7083e-04	3.0541e-02
512	4.2951e-05	1.7655e-02	4.2889e-05	1.7655e-02
1024	1.0735e-05	9.9609e-03	1.0731e-05	9.9609e-03

Table 1: Absolute errors $\|\vec{X} - \vec{x}\|_{L^\infty}$ for the test problem, with $T = \frac{1}{2}\overline{T} = 0.25$ and $T = \overline{T} - \tau$, respectively.

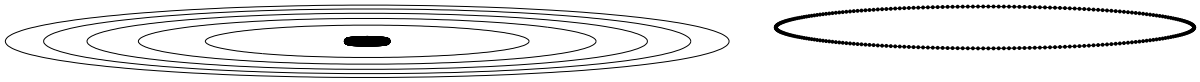

Figure 16: $\vec{X}(t)$ for the convergence test in Table 1 at times $t = 0,\ 0.1,\ 0.2,\ 0.3,\ 0.4,\ T = \overline{T} - \tau$ and $\vec{X}(T)$ (scaled).

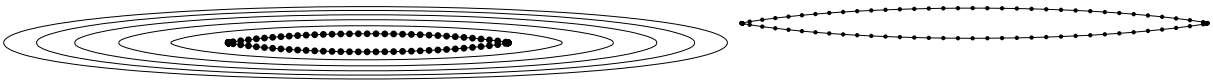

Figure 17: The evolution from Figure 16 now for the scheme (2.19).

singularity is $O(h^2)$, and up to the singularity at time $\overline{T}$ is of order less than $O(h)$, as is to be expected. A plot of the evolution for $N = 256$ and $\varepsilon = 0.1$ can be seen in Figure 16. In comparison, the same evolution for the scheme (2.19) can be seen in Figure 17, where the clustering of mesh points is apparent. This is further underlined by the plot of the ratio r_γ in Figure 18.

We remark that the CPU time for our scheme (2.21) for this last computation was 12 seconds when using the preconditioner (3.1), and 50 seconds without it. The maximal iteration numbers were 187 and 930, respectively.

3.1.3 Inverse anisotropic mean curvature flow

Here we present an experiment for the approximation (2.5), (2.2b) with $f(r) = -r^{-1}$. The corresponding discrete nonlinear system arising at each time step can be solved with a damped Newton method, see Barrett, Garcke, and Nürnberg (2006a). In Figure 19 we show the evolution of a 3:1 ellipse under the inverse anisotropic mean curvature flow for the same anisotropies as in Figure 12. Using the same discretization parameters we can see that, as expected, the ellipse evolves to expanding Wulff shapes.

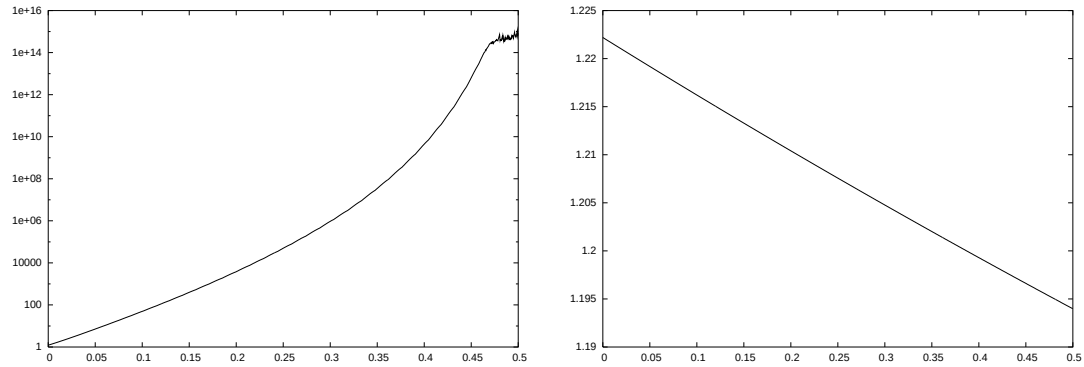

Figure 18: A plot of $\log r_\gamma$ for the scheme (2.19) (left) and a plot of r_γ for (2.21) (right).

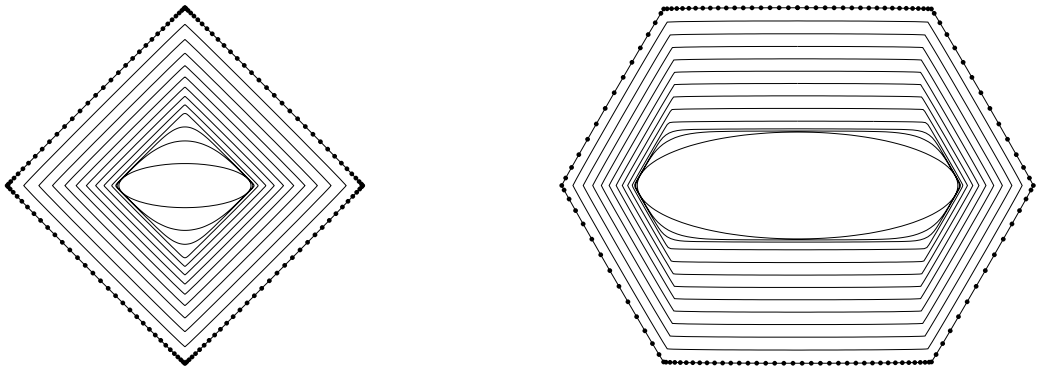

Figure 19: $\vec{X}(t)$ at times $t = 0,\ 0.02,\ 0.04,\ 0.1,\ 0.2, \ldots, T = 1.0$.

3.1.4 Anisotropic intermediate evolution law

In this subsection, we report on numerical results for our approximation (2.25a,b), (2.2b) of the intermediate evolution law (1.19). We compare the different evolutions of (1.10b), (1.17) and (1.18) with $\alpha = \xi = 1$, for an initial curve that is given by an elongated tube of dimensions 10×1. As an anisotropy we chose (1.7) with $(\theta_1, \theta_2) = (\frac{\pi}{4}, \frac{3\pi}{4})$ and $\varepsilon_\ell^2 \equiv 10^{-3}$, while the discretization parameters for the schemes (i) (2.3), (ii) (2.4) and (iii) (2.25a,b), where all are supplemented with (2.2b), were $N = 256$, $\tau = 10^{-3}$ and $T = 20$. The corresponding results are shown in Figure 20. Note that a suitable choice for κ_γ^m in (2.4) for $m = 0$ is given by

$$\kappa_\gamma^0 := -(\vec{N_0}^T \vec{N_0})^{-1} \vec{N_0}^T \vec{A_0}\, \vec{X}^0\,,$$

where we recall the notation from (2.13a,b). The relative area losses for the respective schemes were 0.067%, −0.032% and 0.014%. Furthermore, we give a plot of $|\Gamma(t)|_\gamma$ over time in each case in the same figure. We remark that the results for the area preserving anisotropic mean curvature flow show some small wrinkles close to the sharp corners of the curve at times during the evolution. These are numerical artefacts caused by the two long facets of the curve that are not aligned with the facets of the nearly polygonal Wulff shape, resulting in large jumps in κ_γ^m. Of course, we have no stability result for the approximation (2.4), (2.2b). However, we note that these wrinkles disappear as $h \to 0$; see Dziuk (1999a, p. 1829) for a similar phenomenon. Hence we conjecture that the area preserving anisotropic mean curvature flow preserves convexity in general. For a result in this direction for the isotropic case we refer to Huisken (1987).

3.1.5 Crystalline surface diffusion

In this subsection, we report on numerical experiments that approximate motion by crystalline surface diffusion, see e.g. Taylor (1996) and Taylor (2002). To this end, we used the anisotropy (1.4) with $\varepsilon^2 = 10^{-5}$. An evolution for an initial rectangle with side lengths 3×1 can be seen in Figure 21, where we plot $\vec{X}$ at different times for a computation of (2.3), (2.2b) with $N = 100$ and $\tau = 10^{-3}$. An evolution, during which new facets appear,

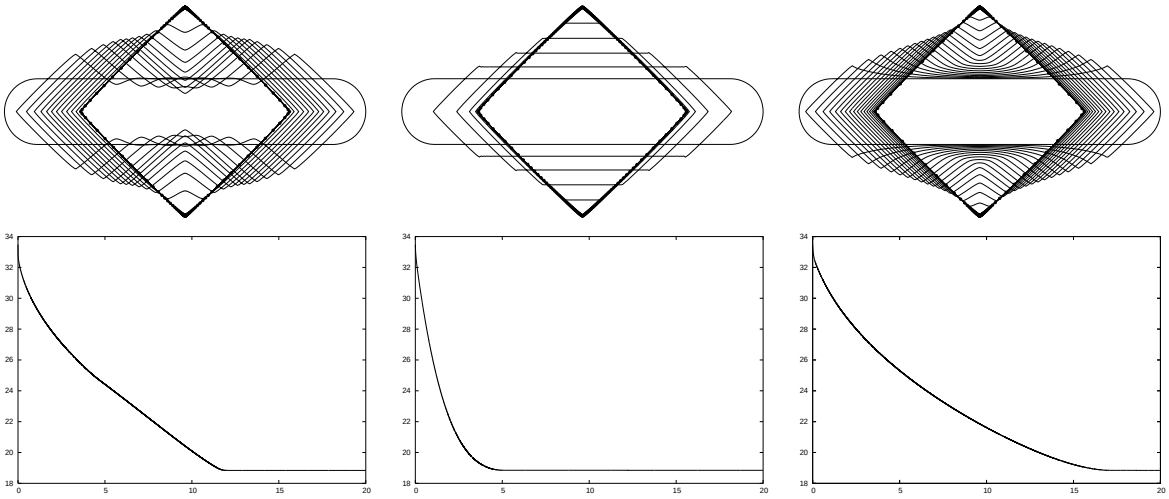

Figure 20: Different evolutions for anisotropic surface diffusion, area preserving anisotropic mean curvature flow (SALK) and the anisotropic intermediate flow (1.19) (with $\alpha = \xi = 1$). In each case, we plot $\vec{X}(t)$ for $t = 0,\ 1, \ldots, T = 20$ and $|\Gamma(t)|_\gamma$ for $t \in [0, T]$.

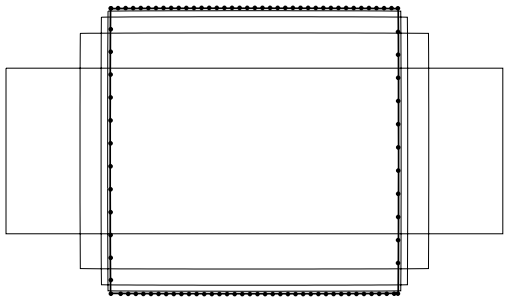

Figure 21: A plot of $\vec{X}(t)$ for $t = 0,\ 0.2, \ldots, T = 1$.

for an initial rectangle with side lengths 20×1 can be seen in Figure 22, where we plot $\vec{X}(t)$, $t = 0, 5, \ldots, 20, T = 50$ for a computation of (2.3), (2.2b) with $N = 200$ and $\tau = 10^{-3}$. The plot of $\vec{X}(T)$ in the same figure shows that there are only very few mesh points on the left and right facet of the Wulff shape. An experiment for an initial letter C, with dimensions $\frac{5}{8} \times \frac{5}{8}$ and "thickness" $\frac{1}{8}$, is shown in Figure 23. Here we used $N = 100$, $\tau = 10^{-6}$ and $T = 3 \times 10^{-3}$. We also show a plot of the energy $|\Gamma(t)|_\gamma$ and note that at time T, the isotropic ratio $r(T) := \max_{j=1 \to N} |\vec{X}^M(q_j) - \vec{X}^M(q_{j-1})| / \min_{j=1 \to N} |\vec{X}^M(q_j) - \vec{X}^M(q_{j-1})|$ has reached a value of 1354.9. This is due to the coalescence of mesh points in the corners of the approximatively polygonal Wulff shape.

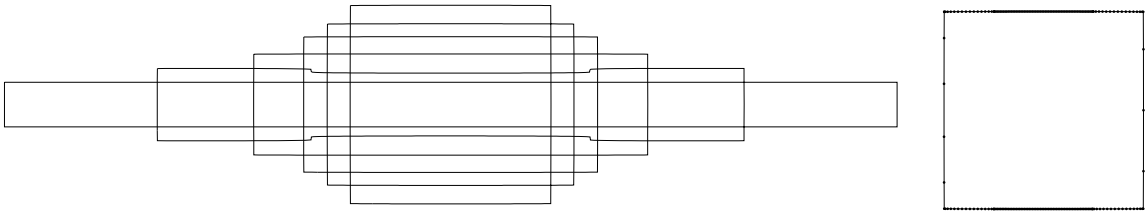

Figure 22: A plot of $\vec{X}(t)$ for $t = 0,\ 5, \ldots, 20,\ T = 50$ and $\vec{X}(T)$.

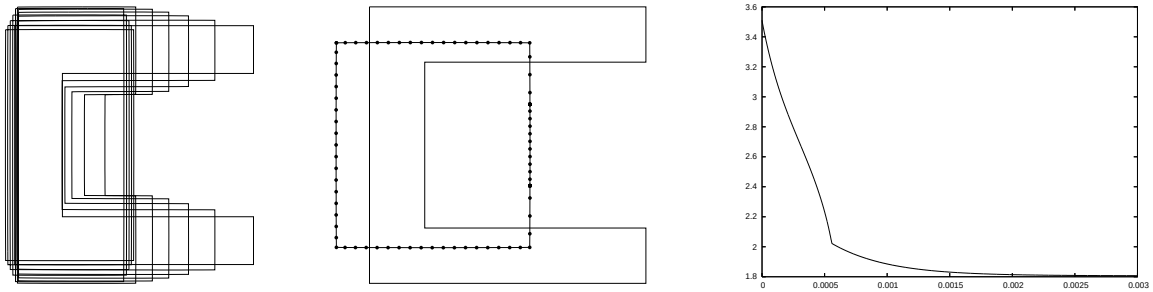

Figure 23: An initial letter C experiment. $\vec{X}(t)$ for $t = 0,\ 10^{-4}, \ldots, 10^{-3}$ (left), $t = 0,\ T$ (middle) and $|\Gamma(t)|_\gamma$ for $t \in [0, T]$.

3.2 Triple junctions

3.2.1 Anisotropic surface diffusion

In all of the following experiments, we report on numerical results for our approximation (2.31a,b). In the first experiment for triple junctions, we simulate how the standard double bubble shape, i.e. a setup where Γ_2 is a straight line and Γ_1 is the arc of a circle with Γ_3 its reflection, see Hutchings, Morgan, Ritoré, and Ros (2002); evolves for different anisotropies. In Figure 24, we use (1.7) with $L = 1$, $\theta_1 = 0$ and $\varepsilon_1^2 = 0.5,\ 0.1,\ 0.01$ so that the eventual steady states represent elliptic double bubbles, similarly to the Wulff shape in the closed curve case. The discretization parameters were $N = 128$, $\tau = 10^{-3}$ and $T = 4$. The observed angles $\vartheta := (\vartheta_1, \vartheta_2, \vartheta_3)$ at the triple junction were $\vartheta = (110.4, 139.2, 110.4)$, $(99.4, 161.2, 99.4)$ and $(93, 174.1, 93)$, respectively. Here ϑ is defined as the angles formed by the three curve segments meeting at a triple junction and ϑ_i, $i = 1 \to 3$, denotes the angle opposite the curve Γ_i^M at a triple junction.

We note that these steady state solutions are unstable. This is demonstrated by the following experiment, where we tilt the initial standard double bubble profile by 5°. The evolution shows that the curves now attain a different numerical steady state which has a lower free energy. See Figure 25 for the results, where we used the same discretization parameters as before. The observed angles at the triple junction were $\vartheta = (115.3, 138.9, 105.8)$, $(148.4, 155.8, 55.8)$ and $(79.1, 107.8, 173.1)$, respectively. As the evolution in the last case is quite interesting, we give some more details in Figure 26.

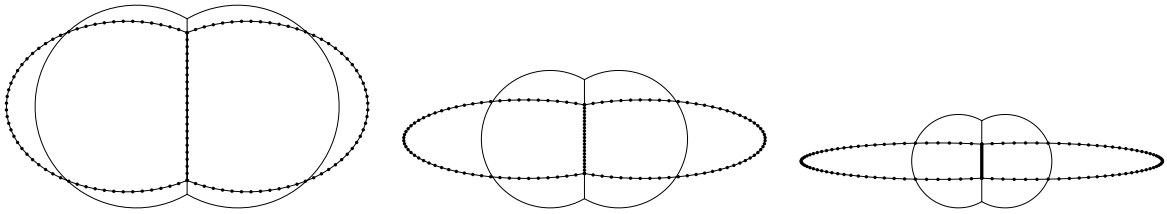

Figure 24: The standard double bubble evolves to its (unstable) anisotropic counterparts.

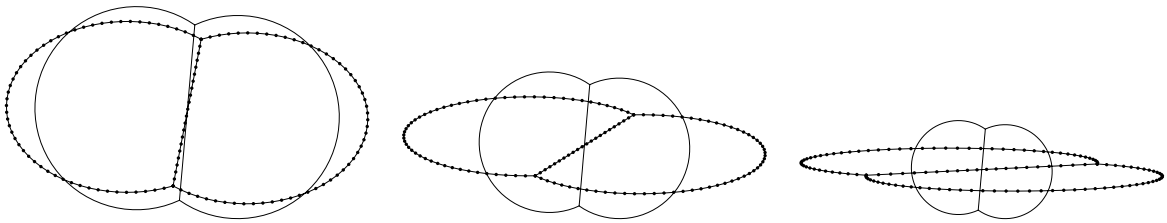

Figure 25: The 5° tilted standard double bubble evolves to numerical steady state solutions.

It is interesting to note that the numerical steady states obtained in Figure 25 are not necessarily the global surface energy minimizers for the given anisotropies. We indicate this with a further set of experiments, where this time the tilt of the initial double bubble is 20°, see Figure 27. For $\varepsilon_1^2 = 0.5$, the steady state shapes in Figures 24, 25 and 27 have total energies of $|\Gamma^M|_\gamma = 8.49932$, 8.49931 and 8.49922 (here and throughout rounded to the displayed number of digits), respectively, i.e. the latter configuration is the one with the smallest free energy. Similarly, for $\varepsilon_1^2 = 0.1$, the energies are $|\Gamma^M|_\gamma = 5.6852$, 5.6850 and 5.6828, with the latter value again being the minimum of the observed values. On the other hand, for $\varepsilon_1^2 = 0.01$, the observed values are $|\Gamma^M|_\gamma = 3.1966$, 3.1890 and 3.1901, i.e. this time the second configuration has the smallest free energy. These examples seem to indicate that for anisotropic surface energies more than one stable double bubble exists in the plane. For isotropic energies it is known that the standard double bubble is the unique double bubble in $\mathbb{R}^2$, see Morgan and Wichiramala (2002).

An example for each of the anisotropies (1.7) with $\varepsilon_\ell^2 \equiv 10^{-3}$ and $(\theta_1, \ldots, \theta_L) = (0, \frac{\pi}{2})$,

Figure 26: $\vec{X}(t)$ at times $t = 0,\ 0.5,\ 1,\ T = 4$ for $\varepsilon_1^2 = 10^{-2}$.

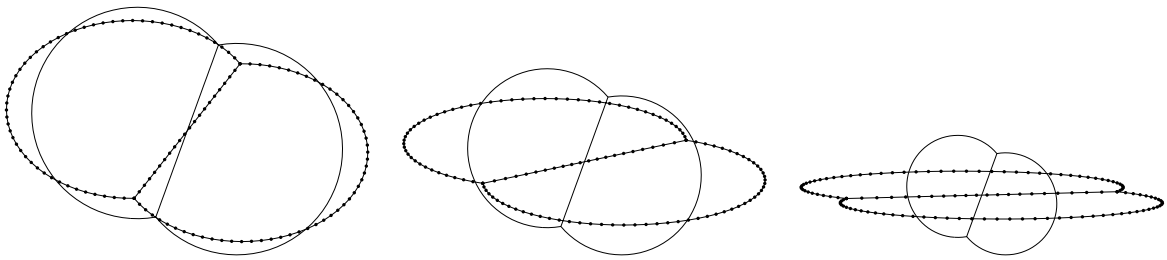

Figure 27: The 20° tilted standard double bubble evolves to numerical steady state solutions.

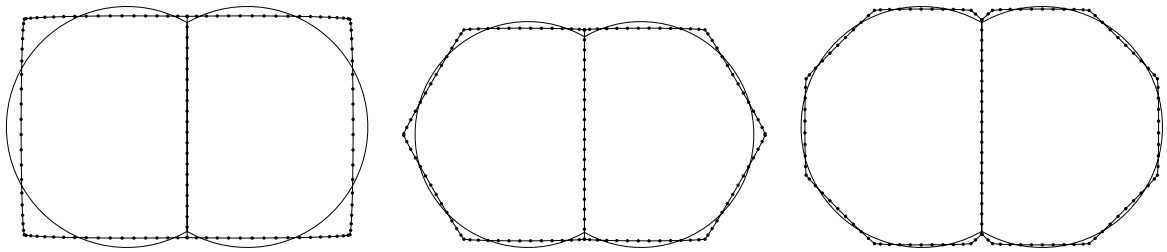

Figure 28: The standard double bubble evolves to its anisotropic counterparts.

$(0, \frac{\pi}{3}, \frac{2\pi}{3})$ or $(0, \frac{\pi}{4}, \frac{\pi}{2}, \frac{3\pi}{4})$ can be seen in Figure 28, where the initial shape is again the standard double bubble, which would be a steady state solution in the isotropic case. The discretization parameters were $N = 128$, $\tau = 10^{-3}$ and $T = 0.5$. The observed angles at the triple junction were $\vartheta = (91, 178.1, 91)$, $(96.1, 167.9, 96.1)$ and $(132.6, 94.8, 132.6)$. We note once again that the orientation of the initial standard double bubble can have an influence on the eventual steady state solution. To demonstrate this, we start the next experiment with an initial standard double bubble that is tilted by 20°, which would again be a steady state solution in the isotropic case. The chosen anisotropies and discretization parameters are as before, except that now $T = 2$. See Figure 29 for the results, where we see that in each case the double bubble aligns itself to the Wulff shape of the given anisotropy. A non-equal area version of the results in Figure 28 can be seen in Figure 30, where we started with an initial setup that consists of a semi-circle and a semi-ellipse with semi major axis 3. We note that in some computations a very non-uniform distribution of vertices can be observed, with nodes clustered in some regions, while only a few vertices are present on other parts of the curves. This is due to the lack of (equidistributing)

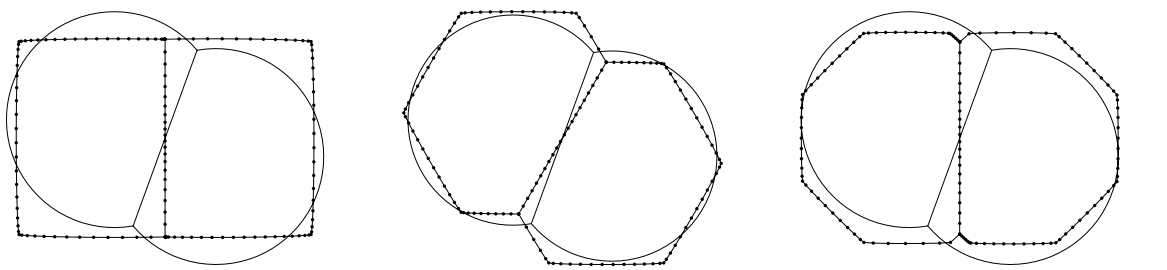

Figure 29: The standard double bubble evolves to its anisotropic counterparts.

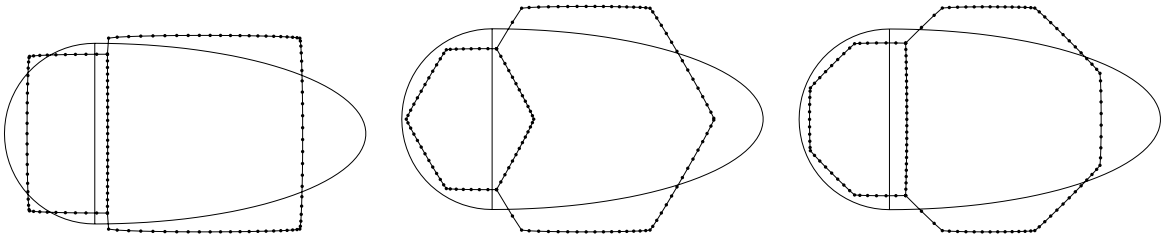

Figure 30: Some non-equal area double bubbles.

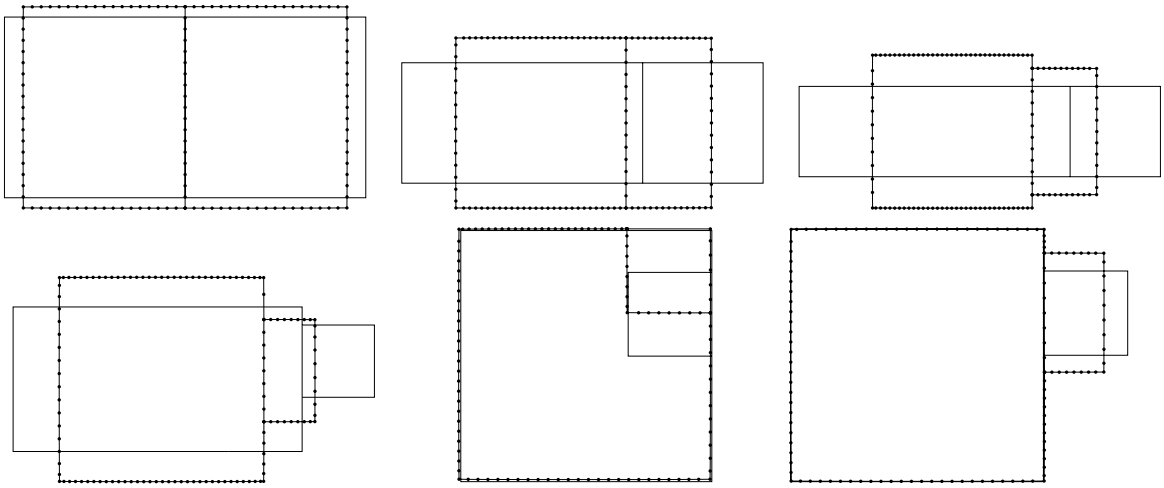

Figure 31: The three different types of energy minimizing double crystals; $R = 1,\ 2,\ 3,\ 8,\ 8,\ 9$.

tangential movement for complicated anisotropies, as discussed in Remark 2.5. In particular, for anisotropies with almost polygonal Wulff shapes we observe almost no tangential movement at all, as the facets of the curves are basically straight leading to locally parallel intervals. We note once again that it is in these situations, that the preconditioner (3.2) improves the efficiency of the conjugate gradient solver for (2.35) considerably.

Of particular interest are the possible steady states in the case of crystalline surface diffusion. These energy minimizers can be observed in real life, e.g. in salt crystals, and the three possible types were categorized in Morgan (1998), see also Wecht, Barber, and Tice (2000). We investigated this problem numerically, by starting with two bubbles, where one is a unit square, and the other is a rectangle with area R, e.g. of dimension $R \times 1$ or $\frac{R}{2} \times 2$. It turns out that the three different types of energy minimizers correspond to the cases $R \leq 2$, $2 < R \leq \mu := \frac{43+30\,2^{\frac{1}{2}}}{16} \approx 5.34$ and $R \geq \mu$, respectively. For our computations, we used the anisotropy (1.7) with $\varepsilon_\ell^2 \equiv 10^{-5}$ and $(\theta_1, \theta_2) = (0, \frac{\pi}{2})$. The discretization parameters were $N = 128$, $\tau = 10^{-3}$ and $T = 50$. The results for $R \in \{1, 2, 3, 8\}$ can be seen in Figure 31, where in each case we plot $\vec{X}(0)$ and the numerical steady state $\vec{X}(T)$. Note that for $R = 8$ we observe two different types of numerical steady states, where

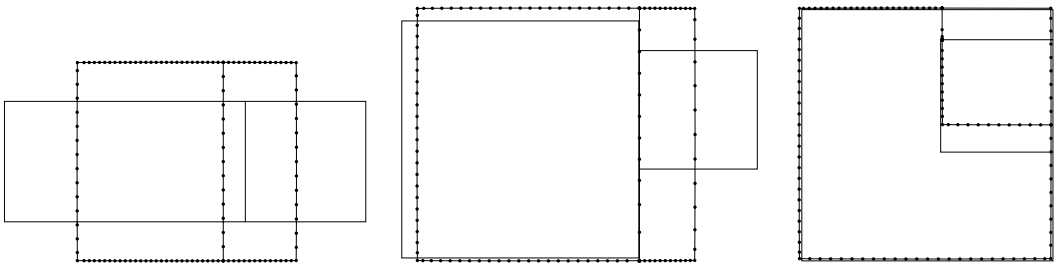

Figure 32: The two different types of energy minimizing double crystals when $\lambda = 0.2$; $R = 2,\ 4,\ 4$.

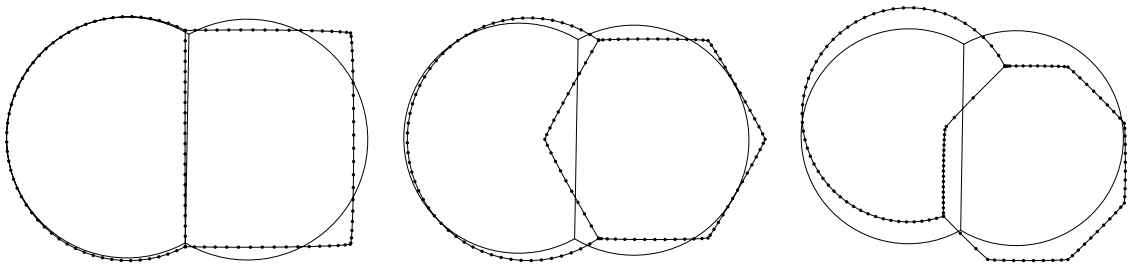

Figure 33: Anisotropic double bubbles with isotropic surface energy on Γ_1.

only the experiment that started from a square inside a square yields the global energy minimizer that is predicted by the theory. This is underlined by the fact that even if we start with the unit square next to a square of area 9, the evolution does not attain the global minimizer.

Moreover, the regime of the energy minimizers changes, if one prescribes differently weighted surface energies on the three curves. Let $\gamma_1 = \gamma_2 = \gamma_0$ as before, and set $\gamma_3(\vec{p}) = \lambda\,\gamma_0(\vec{p})$, where $\lambda \in (0, 1]$ is a weighting factor. Then, for $\lambda > \lambda_0 \approx 0.56$, the three types of minimizing configurations now correspond to the cases $R \leq \frac{2}{\lambda}$, $\frac{2}{\lambda} < R \leq \mu_\lambda$ and $R > \mu_\lambda$, respectively. For $\lambda \leq \lambda_0$, however, the second type disappears and the cut-off value R_λ between the two remaining regimes depends on λ, see Wecht, Barber, and Tice (2000, Figure 4) for more details. As an example, we present two computations for $\lambda = 0.2$ in Figure 32, where we used the ratios $R = 2$ and $R = 4$ and the same discretization parameters as before. We observe once more that the global energy minimizer is only attained when starting from the appropriate initial setup. We note that without a preconditioner, the computation for the last experiment took 7 hours and 11 minutes. With the preconditioner (3.2) for the system (2.35), on the other hand, this was reduced to 33 minutes.

Next we give some computations for double bubbles, where the anisotropies for the three curves differ. In Figure 33 we show results for $\gamma_1(\cdot) = |\cdot|$ and $\gamma_2 = \gamma_3$ as in (1.7) with the parameters as in Figure 28, while in Figure 34 we show results for $\gamma_1(\cdot) = \gamma_2(\cdot) = |\cdot|$ and γ_3 as before, for the first two choices of anisotropy. All of these and the remaining plots show numerical steady states.

We now give some experiments for curve networks with three or more enclosed areas.

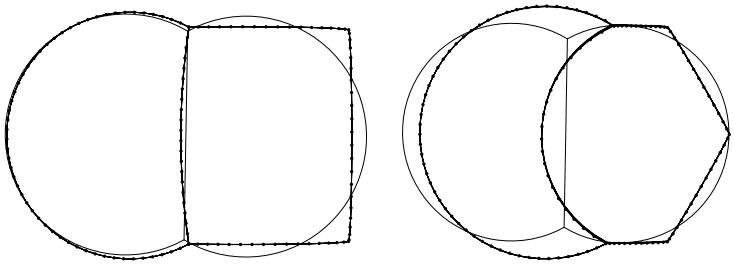

Figure 34: Anisotropic double bubbles with isotropic surface energy on Γ_1 and Γ_2.

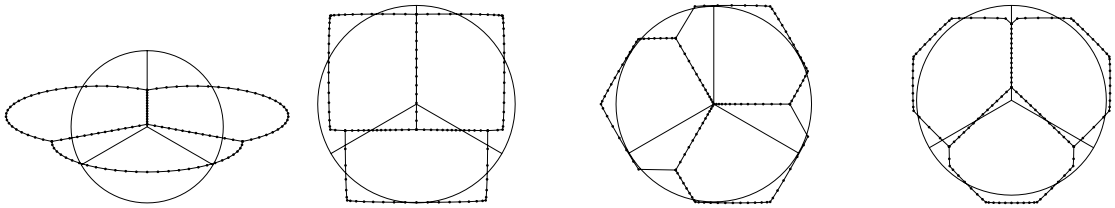

Figure 35: Triple bubble solutions for different anisotropies.

In Figure 35 we show the numerical steady state solutions for triple bubbles with different anisotropies. Here we used (1.7) with $L = 1$, $\theta_1 = 0$ and $\varepsilon_1^2 = 0.1$, as well as (1.7) with $\varepsilon_\ell^2 \equiv 10^{-3}$ and $(\theta_1, \dots, \theta_L) = (0, \frac{\pi}{2})$, $(0, \frac{\pi}{3}, \frac{2\pi}{3})$ or $(0, \frac{\pi}{4}, \frac{\pi}{2}, \frac{3\pi}{4})$. The discretization parameters were $N = 128$, $\tau = 10^{-3}$ and $T = 2$. For the readers convenience, we give a more detailed account of the noteworthy evolution in the case of the last but one chosen anisotropy; see Figure 36.

In Figure 37 we show the numerical steady state solutions for quadruple bubbles for the same anisotropies as in Figure 35. The discretization parameters were $N = 128$, $\tau = 10^{-3}$ and $T = 0.5$.

3.3 Boundary intersections

Here we investigate the evolution of a semi-circle that is attached to the boundary of a rectangular domain under motion by anisotropic surface diffusion, (2.37a,b). An example for each of the anisotropies (1.7) with $L = 1$, $\theta_1 = 0$ and $\varepsilon_1^2 = 0.1$ as well as $\varepsilon_\ell^2 \equiv 10^{-3}$

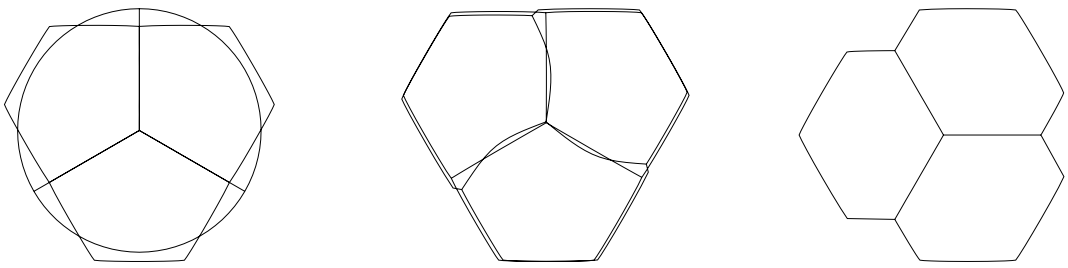

Figure 36: $\vec{X}(t)$ at times $t = 0,\ 0.2$, $t = 1.4,\ 1.6$ and $t = 2$ (from left to right).

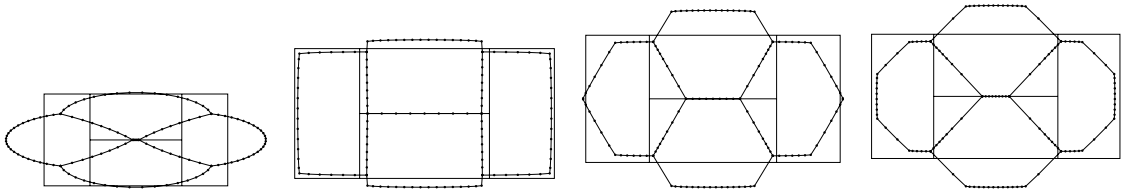

Figure 37: Quadruple bubble solutions for different anisotropies.

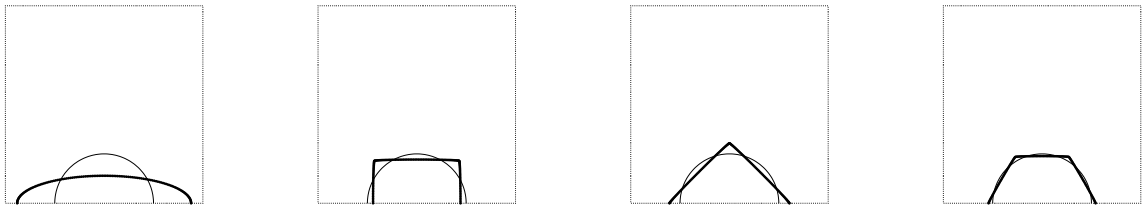

Figure 38: A semi-circle evolves to its anisotropic steady state.

and $(\theta_1, \ldots, \theta_L) = (0, \frac{\pi}{2})$, $(\frac{\pi}{2}, \frac{3\pi}{4})$ or $(0, \frac{\pi}{3}, \frac{2\pi}{3})$ can be seen in Figure 38. The discretization parameters were $N = 128$, $\tau = 10^{-3}$ and $T = 0.2$.

The same choice of anisotropies, but now for an evolving triple junction inside the unit circle, can be seen in Figure 39. Finally, we repeated the latter three experiments in Figure 38 now for a prescribed contact angle of $\alpha_i = 60^\circ$, $i = 1 \to 3$, see Figure 40.

4 Conclusions

We have presented a fully practical parametric finite element approximation for the anisotropic mean curvature flow and anisotropic surface diffusion of curves in $\mathbb{R}^2$ and proved stability bounds. Although there exist stability results for semi-discrete schemes for anisotropic mean curvature flow, see e.g. Dziuk (1999a), we are not aware of any stability result for fully discrete parametric schemes for these anisotropic motion laws in the literature. Moreover, our scheme can also be used to model the evolution of curve networks, where different curves can meet at triple junctions points or intersect the external boundary $\partial\Omega$. Furthermore, the presented scheme intrinsically moves the vertices

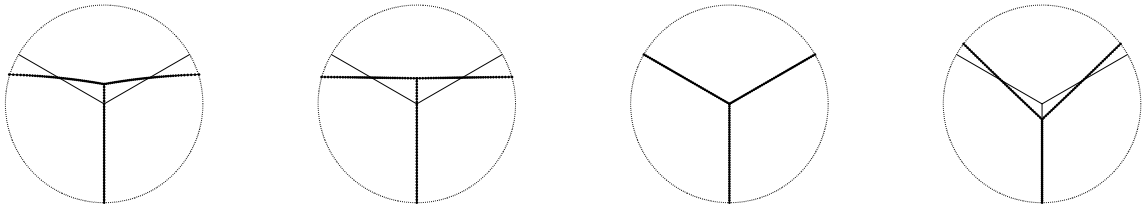

Figure 39: A triple junction inside the unit circle.

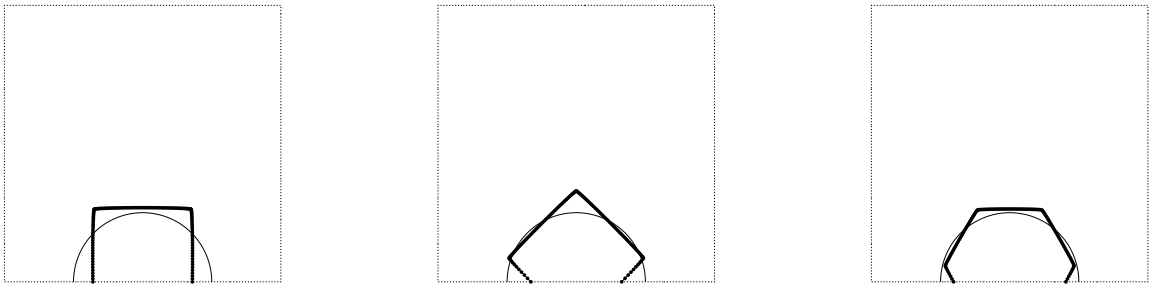

Figure 40: Anisotropic steady state solutions with prescribed boundary contact angle.

tangentially along the curves, so that no artificial redistribution of vertices is necessary in practice.

We remark that extending the presented scheme to the case of 2-dimensional hypersurfaces in $\mathbb{R}^3$ will be part of our ongoing research in this area.

References

Angenent, S. and M. E. Gurtin (1989). Multiphase thermomechanics with interfacial structure. II. Evolution of an isothermal interface. *Arch. Rational Mech. Anal. 108*(4), 323–391.

Bänsch, E., P. Morin, and R. H. Nochetto (2005). A finite element method for surface diffusion: the parametric case. *J. Comput. Phys. 203*(1), 321–343.

Barrett, J. W., H. Garcke, and R. Nürnberg (2005). A parametric finite element method for fourth order geometric evolution equations. Preprint No. 20/2005, University Regensburg.

Barrett, J. W., H. Garcke, and R. Nürnberg (2006a). On the variational approximation of combined second and fourth order geometric evolution equations. Preprint No. 07/2006, University Regensburg.

Barrett, J. W., H. Garcke, and R. Nürnberg (2006b). Phase field models for stress and electromigration induced surface diffusion with applications to epitaxial growth and void evolution. (in preparation).

Bellettini, G. and M. Paolini (1996). Anisotropic motion by mean curvature in the context of Finsler geometry. *Hokkaido Math. J. 25*(3), 537–566.

Cahn, J. W. and D. W. Hoffmann (1974). A vector thermodynamics for anisotropic surfaces – II. curved and faceted surfaces. *Acta Metall. 22*, 1205–1214.

Chopp, D. L. and J. A. Sethian (1999). Motion by intrinsic Laplacian of curvature. *Interfaces Free Bound. 1*, 107–123.

Clarenz, U., G. Dziuk, and M. Rumpf (2003). On generalized mean curvature flow in

surface processing. In *Geometric analysis and nonlinear partial differential equations*, pp. 217–248. Berlin: Springer.

Clarenz, U., F. Haußer, M. Rumpf, A. Voigt, and U. Weikard (2005). On level set formulations for anisotropic mean curvature flow and surface diffusion. In *Multiscale modeling in epitaxial growth*, Volume 149 of *Internat. Ser. Numer. Math.*, pp. 227–237. Basel: Birkhäuser.

Deckelnick, K. and G. Dziuk (2003). A finite element level set method for anisotropic mean curvature flow with space dependent weight. In *Geometric analysis and nonlinear partial differential equations*, pp. 249–264. Berlin: Springer.

Deckelnick, K., G. Dziuk, and C. M. Elliott (2005a). Computation of geometric partial differential equations and mean curvature flow. *Acta Numer. 14*, 139–232.

Deckelnick, K., G. Dziuk, and C. M. Elliott (2005b). Fully discrete finite element approximation for anisotropic surface diffusion of graphs. *SIAM J. Numer. Anal. 43*(3), 1112–1138.

Di Carlo, A., M. E. Gurtin, and P. Podio-Guidugli (1992). A regularized equation for anisotropic motion-by-curvature. *SIAM J. Appl. Math. 52*(4), 1111–1119.

Dziuk, G. (1999a). Discrete anisotropic curve shortening flow. *SIAM J. Numer. Anal. 36*, 1808–1830.

Dziuk, G. (1999b). Numerical schemes for the mean curvature flow of graphs. In *Variations of domain and free-boundary problems in solid mechanics (Paris, 1997)*, Volume 66 of *Solid Mech. Appl.*, pp. 63–70. Dordrecht: Kluwer Acad. Publ.

Elliott, C. M. and H. Garcke (1997). Existence results for diffusive surface motion laws. *Adv. Math. Sci. Appl. 7*, 465–488.

Frank, C. (1963). The geometrical thermodynamics of surfaces. *Amer. Soc. Metals*, 1–15. In Metal Surfaces: Structure, Energies, and Kinetics.

Garcke, H., B. Nestler, and B. Stoth (1999). Anisotropy in multi phase systems: a phase field approach. *Interfaces and Free Bound. 1*, 175–198.

Garcke, H. and A. Novick-Cohen (2000). A singular limit for a system of degenerate Cahn–Hilliard equations. *Adv. Differential Equations 5*, 401–434.

Giga, Y. (2006). *Surface Evolution Equations*. Basel, Boston, Berlin: Birkhäuser.

Girão, P. M. (1995). Convergence of a crystalline algorithm for the motion of a simple closed convex curve by weighted curvature. *SIAM J. Numer. Anal. 32*(3), 886–899.

Gurtin, M. E. (1993). *Thermomechanics of Evolving Phase Boundaries in the Plane*. New York: Oxford University Press.

Haußer, F. and A. Voigt (2005). A discrete scheme for regularized anisotropic surface diffusion: a 6th order geometric evolution equation. *Interfaces Free Bound. 7*, 353–369.

Haußer, F. and A. Voigt (2006). A discrete scheme for regularized anisotropic curve shortening flow. *Appl. Math. Lett.*. (to appear).

Herring, C. (1951). Surface tension as a motivation for sintering. In W. E. Kingston (Ed.), *The Physics of Powder Metallurgy*, pp. 143–179. New York: McGraw–Hill.

Huisken, G. (1987). The volume preserving mean curvature flow. *J. Reine Angew. Math. 382*, 35–48.

Hutchings, M., F. Morgan, M. Ritoré, and A. Ros (2002). Proof of the double bubble conjecture. *Ann. of Math. (2) 155*(2), 459–489.

Morgan, F. (1998). *Riemannian geometry* (Second ed.). Wellesley, MA: A K Peters Ltd. A beginner's guide.

Morgan, F. and W. Wichiramala (2002). The standard double bubble is the unique stable double bubble in $\mathbb{R}^2$. *Proc. Amer. Math. Soc. 130*(9), 2745–2751.

Peng, D., S. Osher, B. Merriman, and H.-K. Zhao (1999). The geometry of Wulff crystal shapes and its relations with Riemann problems. In *Nonlinear partial differential equations (Evanston, IL, 1998)*, Volume 238 of *Contemp. Math.*, pp. 251–303. Providence, RI: Amer. Math. Soc.

Russo, G. and P. Smereka (2000). A level-set method for the evolution of faceted crystals. *SIAM J. Sci. Comput. 21*(6), 2073–2095.

Soner, H. M. (1993). Motion of a set by the curvature of its boundary. *J. Differential Equations 101*(2), 313–372.

Taylor, J. E. (1988). Constructions and conjectures in crystalline nondifferential geometry. In *Proceedings of the Conference on Differential Geometry*, London. Pitman.

Taylor, J. E. (1992). Mean curvature and weighted mean curvature. *Acta Metall. 40*, 1475–1485.

Taylor, J. E. (1993). Motion of curves by crystalline curvature, including triple junctions and boundary points. In *Differential geometry: partial differential equations on manifolds (Los Angeles, CA, 1990)*, Volume 54 of *Proc. Sympos. Pure Math.*, pp. 417–438. Providence, RI: Amer. Math. Soc.

Taylor, J. E. (1996). Surface motion due to crystalline surface energy gradient flows. In *Elliptic and parabolic methods in geometry (Minneapolis, MN, 1994)*, pp. 145–162. Wellesley, MA: A K Peters.

Taylor, J. E. (1999). A variational approach to crystalline triple-junction motion. *J. Statist. Phys. 95*(5-6), 1221–1244.

Taylor, J. E. (2002). Crystalline variational methods. *Proc. Natl. Acad. Sci. USA 99*(24), 15277–15280.

Taylor, J. E. and J. W. Cahn (1994). Linking anisotropic sharp and diffuse surface motion laws via gradient flows. *J. Statist. Phys. 77*, 183–197.

Taylor, J. E., J. W. Cahn, and C. A. Handwerker (1992). Geometric models of crystal growth. *Acta Metall. Mater. 40*, 1443–1474.

Wecht, B., M. Barber, and J. Tice (2000). Double crystals. *Acta Cryst. Sect. A 56*(1), 92–95.

Wulff, G. (1901). Zur Frage der Geschwindigkeit des Wachstums und der Auflösung der Kristallflächen. *Z. Krist. 34*, 449–530.